



The cells and conductance mediating cholinergic neurotransmission in the murine proximal stomach

Tae Sik Sung^{1,*}, Sung Jin Hwang^{1,*}, Sang Don Koh¹, Yulia Bayguinov¹, Lauen E. Peri¹, Peter J. Blair¹, Timothy I. Webb¹, David M. Pardo², Jason R. Rock³, Kenton M. Sanders¹  and Sean M. Ward¹ 

¹Department of Physiology and Cell Biology, University of Nevada, Reno School of Medicine, Reno, NV, USA

²Department of Anatomy, University of California, San Francisco, CA, USA

³Center for Regenerative Medicine, Boston University School of Medicine, Boston, MA, USA

Edited by: Peying Fong & Keith Sharkey

Key points

- Enteric neurotransmission is essential for gastrointestinal (GI) motility, although the cells and conductances responsible for post-junctional responses are controversial.
- The calcium-activated chloride conductance (CaCC), anoctamin-1 (Ano1), was expressed by intramuscular interstitial cells of Cajal (ICC-IM) in proximal stomach and not resolved in smooth muscle cells (SMCs).
- Cholinergic nerve fibres were closely apposed to ICC-IM.
- Conductances activated by cholinergic stimulation in isolated ICC-IM and SMCs were determined. A CaCC was activated by carbachol in ICC-IM and a non-selective cation conductance in SMCs.
- Responses to cholinergic nerve stimulation were studied. Excitatory junction potentials (EJPs) and mechanical responses were evoked in wild-type mice but absent or greatly reduced with knockout/down of Ano1.
- Drugs that block Ano1 inhibited the conductance activated by carbachol in ICC-IM and EJPs and mechanical responses in tissues.
- The data of the present study suggest that electrical and mechanical responses to cholinergic nerve stimulation are mediated by Ano1 expressed in ICC-IM and not SMCs.

Abstract Enteric motor neurotransmission is essential for normal gastrointestinal (GI) motility. Controversy exists regarding the cells and ionic conductance(s) that mediate post-junctional neuroeffector responses to motor neurotransmitters. Isolated intramuscular ICC (ICC-IM) and smooth muscle cells (SMCs) from murine fundus muscles were used to determine the conductances activated by carbachol (CCh) in each cell type. The calcium-activated chloride conductance (CaCC), anoctamin-1 (Ano1) is expressed by ICC-IM but not resolved in SMCs, and CCh activated a Cl⁻ conductance in ICC-IM and a non-selective cation conductance in SMCs. We also studied responses to nerve stimulation using electrical-field stimulation (EFS) of intact fundus muscles from wild-type and Ano1 knockout mice. EFS activated excitatory junction potentials (EJPs) in wild-type mice, although EJPs were absent in mice with congenital deactivation of Ano1 and greatly reduced in animals in which the CaCC-Ano1 was knocked down using Cre/loxP technology. Contractions to cholinergic nerve stimulation were also greatly reduced in Ano1 knockouts. SMCs cells also have receptors and ion channels activated by muscarinic agonists. Blocking acetylcholine esterase with neostigmine revealed a slow depolarization that

*These authors contributed equally to this work.

developed after EJPs in wild-type mice. This depolarization was still apparent in mice with genetic deactivation of *Ano1*. Pharmacological blockers of *Ano1* also inhibited EJPs and contractile responses to muscarinic stimulation in fundus muscles. The data of the present study are consistent with the hypothesis that ACh released from motor nerves binds muscarinic receptors on ICC-IM with preference and activates *Ano1*. If metabolism of acetylcholine is inhibited, ACh overflows and binds to extrajunctional receptors on SMCs, eliciting a slower depolarization response.

(Received 14 November 2017; accepted after revision 26 January 2018; first published online 12 February 2018)

Corresponding author S. M. Ward: Department of Physiology and Cell Biology, University of Nevada, Reno School of Medicine, Reno, NV 89557, USA. Email: smward@med.unr.edu

Introduction

The smooth muscle/interstitial cells of Cajal (ICC)/platelet-derived growth factor receptor α positive (PDGFR α^+) cell (SIP) syncytium generates spontaneous electrical activity and regulates the excitability of gastrointestinal (GI) smooth muscles (Sanders *et al.* 2014a), although organ-level motility patterns are co-ordinated by the enteric nervous system. An example of this is the gastric accommodation reflex that is mediated by enteric motor neurons innervating the SIP syncytium of the proximal stomach (Desai *et al.* 1991; Tack *et al.* 2002). Previous studies have suggested that motor innervation of the proximal stomach by nitrergic (inhibitory) and cholinergic (excitatory) neurons occurs, in part, through transduction mechanisms expressed by ICC (Burns *et al.* 1996; Ward *et al.* 2000). However, other studies have contested this hypothesis, based on studies of *Kit* mutants in which ICC are developmentally impaired and reduced in numbers, and concluded that ICC are not important for enteric motor neurotransmission (Huizinga *et al.* 2008; Zhang *et al.* 2011).

We have also reported that cholinergic neurotransmission persists in *Kit* mutants, and contractile responses to cholinergic neurotransmission can actually be enhanced in amplitude *vs.* responses in wild-type muscles (Sanders *et al.* 2014b). However, assays of post-junctional Ca²⁺ sensitization pathways demonstrate that loss of ICC causes recruitment of Ca²⁺ sensitization mechanisms that do not appear to be activated by cholinergic neurotransmission in wild-type animals (Bhetwal *et al.* 2013). Thus, although fundus muscles deprived of most ICC respond to cholinergic nerves, these responses are abnormal in nature. The mechanisms responsible for augmented cholinergic responses in *Kit* mutants probably leads to abnormal contractile responses to other hormones, neurotransmitters and paracrine substances because changing the gain of Ca²⁺ sensitivity mechanisms would tend to affect contractile responses to all excitatory and inhibitory agonists. Our studies also showed that the Ca²⁺ sensitization pathway (i.e. CPI-17 phosphorylation) activated in wild-type mice depends upon activation of a Ca²⁺-dependent protein kinase C (PKC), which could

be regulated by a SIP syncytial pathway including: (i) acetylcholine binds to muscarinic receptors on ICC; (ii) activation of an inward current; (iii) conduction of the depolarization response to smooth muscle cells (SMCs); (iv) stimulation of Ca²⁺ entry; and (v) activation of PKC. A better understanding of the post-junctional mechanisms responsible for neuroeffector responses may provide ideas for novel therapies for gastric emptying disorders, gastroparesis and functional dyspepsia.

Cholinergic neurotransmission in GI muscles of several species has long been assumed to be dependent upon activation of a non-selective cation conductance (NSCC) in SMCs (Benham *et al.* 1985; Lim & Bolton, 1988; Inoue & Isenberg, 1990a; Vogalis & Sanders, 1990; Sims, 1992; Lee *et al.* 1993; Zholos & Bolton, 1997). Isolated SMCs express a rectifying, voltage and Ca²⁺-dependent NSCC that is activated through binding of muscarinic receptors (Inoue & Isenberg, 1990b; Pacaud & Bolton, 1991a; Bolton & Zholos, 1997; Gordienko & Zholos, 2004) and more recent studies identified *Trpc4* and *Trpc6* as the genes encoding the transient receptor protein channels mediating cholinergic excitation (Tsvilovskyy *et al.* 2009).

A prominent CaCC (encoded by *Ano1*) has been identified in ICC of GI muscles, including humans (Gomez-Pinilla *et al.* 2009; Hwang *et al.* 2009; Zhu *et al.* 2009, 2011; Rhee *et al.* 2011; Blair *et al.* 2012). *Ano1* is expressed in Kit⁺ ICC, and its gene products, *Ano1* channels, have been implicated in the pacemaker activity of GI muscles (Hwang *et al.* 2009; Zhu *et al.* 2009; Singh *et al.* 2014; Cobine *et al.* 2017; Malysz *et al.* 2017). In the murine stomach, pacemaker activity, attributed to ICC in the plane of the myenteric plexus (ICC-MY), is resolved in the gastric corpus and antrum but typically not observed in the fundus (Burns *et al.* 1996; Ward *et al.* 2000; Beckett *et al.* 2004, 2017) where only intramuscular ICC (ICC-IM) are found (Burns *et al.* 1996; Ward *et al.* 2000; Beckett *et al.* 2004). ICC-IM in the fundus make close, synapse-like anatomical contacts with varicosities of enteric motor neurons and form gap junctions with neighbouring SMCs (Horiguchi *et al.* 2003; Beckett *et al.* 2005; Sanders *et al.* 2014a). Thus, responses activated in ICC-IM would be expected to conduct to SMCs. We found previously that cholinergic responses in the small

Table 1. Details of mouse strains utilized

Strain name	Source	Abbreviated name
C57Bl6/J wild-type	The Jackson Laboratory (Bar Harbor, NE, USA)	(+/+)
<i>Ano1</i> ^{+/+} (<i>tm1Bdh</i>)/(<i>tm1Bdh</i>)*	Jason Rock (Boston University, MA, USA)	<i>Ano1</i> ^{+/+}
<i>Ano1</i> ^{-/-} (<i>tm1Bdh</i>)/(<i>tm1Bdh</i>)*	Jason Rock (Boston University, MA, USA)	<i>Ano1</i> ^{-/-}
<i>Kit</i> ^{CreERT2Ejb1/+} (<i>Kit-Cre</i>)	Deiter Sauer (Technical University Munich, Munich, Germany)	<i>Kit</i> ^{CreERT2}
<i>Ano1</i> ^{tm1jrr}	The Jackson Laboratory (Bar Harbor, NE, USA)	<i>iAno1</i> ^{+/-}
<i>Kit</i> ^{CreERT2/+} ; <i>Ano1</i> ^{tm1jrr/+}	University of Nevada (Reno, NV, USA)	<i>iAno1</i> ^{-/-}
<i>Kit</i> ^{CreERT2/+} ; <i>Ano1</i> ^{tm1jrr/-}	University of Nevada (Reno, NV, USA)	<i>mTImG</i>
<i>Gt(ROSA)26Sor</i> ^{tm4} (<i>ACTB-tdTomato,-EGFP</i>) <i>Luo/J</i>	The Jackson Laboratory (Bar Harbor, NE, USA)	
<i>Kit</i> ^{CreERT2/+} ; <i>Ano1</i> ^{tm1jrr/+} ; <i>Rosa</i> ^{mtmg}	Jason Rock (Boston University, MA, USA)	<i>iAno1</i> ^{+/-} ; <i>Rosa</i>
<i>Kit</i> ^{CreERT2/+} ; <i>Ano1</i> ^{tm1jrr/-} ; <i>Rosa</i> ^{mtmg}	Jason Rock (Boston University, MA, USA)	<i>iAno1</i> ^{-/-} ; <i>Rosa</i>
<i>Kit</i> ^{copGFP/+}	University of Nevada (Reno, NV, USA)	<i>Kit</i> ^{copGFP}
<i>Pdgfra</i> ^{tm11} (<i>EGFP</i>) <i>Sor/J</i>	The Jackson Laboratory (Bar Harbor, NE, USA)	<i>Pdgfra</i> ^{eGFP/+}
<i>B6.Cg-Tg</i> (<i>Myh11-cre,eGFP</i>)	Michel Kotlikoff, Cornell University (Ithaca, NY, USA)	<i>Myh11</i> ^{eGFP/+}

* *Ano1*^{+/+}(*tm1Bdh*)/(*tm1Bdh*) and *Ano1*^{-/-}(*tm1Bdh*)/(*tm1Bdh*) mice were previously termed *Tmem16a*^{+/+}(*tm1Bdh*)/(*tm1Bdh*) and *Tmem16*^{-/-}(*tm1Bdh*)/(*tm1Bdh*) mice respectively.

intestine are linked to activation of a CaCC (Zhu *et al.* 2011). However, the results of that study were based on pharmacological blockade of CaCC using traditional blockers of this conductance, such as niflumic acid, which can have non-specific effects (Hartzell *et al.* 2005).

In the present study, we tested the hypothesis that a CaCC, rather than a NSCC, is the primary conductance activated in post-junctional cells in the proximal stomach during cholinergic neurotransmission. We examined the type(s) of conductances activated by cholinergic nerve stimulation in cells of the murine fundus and then studied cholinergic responses in muscles with *Ano1* deactivated genetically. The results obtained demonstrate that a CaCC-*Ano1* mediates cholinergic excitatory junction potentials (EJPs) and contractions and that knockdown of *Ano1* inhibits electrical and mechanical responses to cholinergic excitatory neurotransmission.

Methods

Animals

Mice were purchased from The Jackson Laboratory (Bar Harbor, ME, USA) or where specific strains were used, generated in house at the University of Nevada (Reno, NV, USA) or University of California San Francisco (San Francisco, CA, USA). Several strains were used, including: (i) *Ano1*^{(tm1Bdh)/(tm1Bdh)} previously termed *Tmem16a*^{(tm1Bdh)/(tm1Bdh)} because these mice die as neonates (Rock *et al.* 2008), they were used by P5; (ii) *Kit*^{CreERT2Ejb1/+} (*Kit*^{CreERT2}) mice were donated by Dr Dieter Sauer (Technical University Munich, Munich, Germany) (Klein *et al.* 2013) and crossed with *Ano1*^{tm1jrr} to generate *Kit*^{CreERT2/+}; *Ano1*^{tm1jrr/+} and *Kit*^{CreERT2/+}; *Ano1*^{tm1jrr/-} animals (Faria *et al.* 2014; Schreiber *et al.*

2015); (iii) *Kit*^{CreERT2/+} mice were also crossed with *Gt(ROSA)26Sor*^{tm4}(*ACTB-tdTomato,-EGFP*)*Luo/J* reporter mice to produce *Kit*^{CreERT2/+}; *Ano1*^{tm1jrr/+}; *Rosa*^{mtmg} and *Kit*^{CreERT2/+}; *Ano1*^{tm1jrr/-}; *Rosa*^{mtmg} animals; (iv) *Kit*^{copGFP/+} mice (P8-P10) were used for patch clamp and molecular expression studies because expression of the reporter allowed unequivocal identification of ICC in a mixed cell population resulting after enzymatic dispersion, as described previously (Zhu *et al.* 2009; Zhu *et al.* 2011); (v) *Pdgfra*^{tm11}(*EGFP*)*Sor/J* heterozygote mice (The Jackson Laboratory), where PDGFR α ⁺ cells are constitutively labelled by expression of a transgene encoding a histone 2B-enhanced green fluorescent protein (eGFP) fusion protein driven by the endogenous, cell-specific *Pdgfra* promoter; these mice were used to purify PDGFR α ⁺ cells by fluorescence-activated cell sorting (FACS); and (vi) *B6.Cg-Tg*^(Myh11-cre,eGFP) mice (*Myh11*^{eGFP/+}; donated by Dr Michael Kotlikoff, Cornell University, Ithaca, New York) were used to identify SMCs for comparative molecular transcript studies. (vii) Age-matched *C57Bl6/J* (The Jackson Laboratory) between the ages post-embryonic day (P)3–P5 and 15 weeks were also used as control mice for morphological and physiological experiments (complete mice information and abbreviated names are provided in Table 1). The animals used in the present study were age-matched and experiments were performed in accordance with the National Institutes of Health Guide for the Care and Use of Laboratory Animals. The Institutional Animal Use and Care Committees at the University of Nevada, Reno and University of California, San Francisco approved the procedures used on the mice. Animals were fed *ad libitum* and had free access to water. Animals were humanely killed by isoflurane sedation followed by cervical dislocation and exsanguination. The investigators involved in the present study are aware of the

Table 2. Details of antibody combinations used for double-label immunohistochemistry

Combined antibodies	Source	Mono- or poly-clonal antibodies	Host	Dilution
mSCFR/TMEM16A*	R&D Systems Inc. (Minneapolis, MN, USA)/Abcam (Cambridge, MA, USA)	Poly-/Poly-	Goat/Rabbit	1:100/1:800
mSCFR/vAChT**	R&D Systems Inc. (Minneapolis, MN, USA)/EMD Millipore Corp. (Temecula, CA, USA)	Poly-/Poly-	Goat/Rabbit	1:100/1:500
eGFP/TMEM16A*	Abcam (Cambridge, MA, USA)/Abcam (Cambridge, MA, USA)	Poly-/Poly-	Chicken/Rabbit	1:1000/1:800

mSCFR, anti-mouse stem cell factor receptor; TMEM16A, anti-anoctamin 1 (Ano1); vAChT, anti-vesicular acetylcholine transporter.
*Gastric tissues fixed in paraformaldehyde. **Gastric tissues fixed in acetone.

ethical principles under which *The Journal of Physiology* operates and confirm that the use of animals presented here complies with the check list in Grundy (2015).

The stomachs from the oesophagus to the pyloric sphincter was removed and placed in oxygenated Krebs-Ringer buffer (KRB) for further dissection. Stomachs were opened along the lesser curvature and gastric contents were washed away with KRB. The gastric fundus was isolated by a surgical incision across the stomach along the border between fundus and corpus (as indicated by a change in the mucosa structure) and processed for morphological or physiological experiments. To induce Cre recombinase, 8-week-old mice were treated with tamoxifen (Sigma-Aldrich, St Louis, MO, USA) by i.p. injection (0.2 mg i.p. injection made up as 20 mg mL⁻¹ solution in safflower oil). Each animal received four consecutive doses of tamoxifen given every other day and the experiments were performed from 7 weeks following the last treatment. This has been reported to be successful with respect to obtaining maximal gene knockdown in the GI tract (Groneberg *et al.* 2015).

Genotyping and phenotyping

Ano1^{(tm1Bdh)/(tm1Bdh)} mice were generated by replacing exon 12 of *Tmem16a* with a phosphoglycerate kinase-neomycin cassette by homologous recombination in embryonic stem cells (Rock *et al.* 2008). Genomic DNA was isolated from transgenic mice tails using standard procedures. DNA (0.5 µL) was amplified in each PCR reaction to determine the genotypes of the transgenic mice. A 393 bp PCR fragment was amplified from the *Tmem16a*^{+/+} allele with primers that bind within and spanning exon 12. The *Ano1*^{-/-} allele (350 bp) was amplified with primers that bind to the PGK-neomycin cassette as described previously (Hwang *et al.* 2009).

Kit^{CreERT2Ejb1/+ (Kit-Cre)} were generated by inserting CreERT2 under control of the mouse proto-oncogene receptor tyrosine kinase (Kit) promoter/enhancer regions on the BAC transgene. Genomic DNA was isolated from

transgenic mice tails using standard procedures. DNA (0.5 µL) was amplified in each PCR reaction to determine the genotypes of the transgenic mice. A 685 bp PCR fragment was amplified from the *Kit*^{CreERT2+/+} allele with primers that span the insertion region. The 330 bp PCR fragment was amplified from the *Kit*^{CreERT2+/-} allele with primers that bind to the CreERT2 insert (Klein *et al.* 2013). When *Kit*^{CreERT2+/-} mice are bred with mice containing loxP-flanked sequence, tamoxifen-inducible, Cre-mediated recombination results in deletion of the floxed sequences in Kit cells of the offspring.

GI tissues from *Pdgfra*^{tm11(EGFP)Sor/J} heterozygotes and *Myh11*^{eGFP/+} mice were phenotyped under a fluorescence microscope for eGFP expression.

Morphological studies

Whole mounts were prepared after removing the mucosa from fundus by sharp dissection. The remaining strips of tunica muscularis were pinned to the base of a dish filled with Sylgard elastomer (Dow Corning Corp., Midland, MI, USA) with the circular muscle layer facing upward and stretched to 110% of their resting length. Tissues were fixed in either acetone (4°C for 10 min) or paraformaldehyde [4% w/v in 0.1 M phosphate buffer (PB) for 15 min at 4°C]. Following fixation, preparations were washed overnight in PBS (0.01 M, pH 7.4). Incubation of tissues in BSA (1%) for 1 h at room temperature containing Triton X-100 (0.3%) was used to reduce non-specific antibody binding. For double-labelling, tissues were incubated sequentially in a combination of primary antibodies (Table 2). The first incubation was carried out for 48 h at 4°C; tissues were subsequently washed in PBS before being incubated in a second antibody for an additional 48 h at 4°C. The combinations of antibodies used were goat/rabbit and chicken/rabbit. Following incubation in primary antibodies, tissues were washed and incubated separately in secondary antibodies (Alexa Fluor 488 and 594; Thermo Fisher Scientific Inc., Waltham, MA, USA, diluted to 1:1000 in PBS for 1 h

at room temperature). Control tissues were prepared by either omitting primary or secondary antibodies from the incubation solutions. Tissues were examined with an LSM 510 Meta confocal microscope (Carl Zeiss, Jena, Germany) with appropriate excitation wavelengths. Confocal micrographs are digital composites of Z-series scans of 10–20 optical sections through a depth of 2–40 μm . Final images were constructed and montages were assembled using LSM 5 Image Examiner (Carl Zeiss) and converted to Tiff files for processing in Photoshop CS5 (Adobe Co., Mountain View, CA, USA) and Corel Draw X4 (Corel Corp., Ottawa, ON, Canada).

Cell purification and cell-specific RNA isolation and quantitative RT-PCR (qRT-PCR)

Strips of gastric fundus muscles (25 ± 5 mg tissue weight) were equilibrated in Ca^{2+} -free Hanks' solution at 4°C consisting of (mM): 125 NaCl, 5.36 KCl, 15.5 NaHCO_3 , 0.336 Na_2HPO_4 , 0.44 KH_2PO_4 , 10 glucose, 2.9 sucrose and 11 Hepes, adjusted to pH 7.2 with NaOH, for 30 min. Cells were dispersed as described previously (Zhu *et al.* 2009). Briefly, muscle strips were incubated for 25 ± 2 min at 37°C in an enzyme solution containing (per mL): 1.0 mg of collagenase (Worthington Type II; Worthington Biochemical, Lakewood, NJ, USA), 2.0 mg of BSA (Sigma, St Louis, MO, USA), 2.0 mg of trypsin inhibitor (Sigma) and 0.13 mg of ATP (Sigma). Strips were washed with Ca^{2+} -free Hanks' solution to remove the enzyme and isolated cells were obtained by triturating the digested tissues. eGFP-SMCs, CopGFP-ICC and eGFP-PDGFR α cells were purified by FACS (FACSARIAII; Becton-Dickinson, Franklin Lakes, NJ, USA) using the blue laser (488 nm) and the GFP emission detector (530/30 nm). Expression of genes in each sorted cell type was compared against expression in the total fundus cell population (TCP). TCP represents all cells dispersed from the tunica muscularis from fundus and was prepared from each cell-specific reporter mouse strain. Gene transcript expression was averaged from three mice of each reporter strain.

Total RNA was isolated from SMCs, ICC and PDGFR α^+ cells, using an illustra RNAspin Mini RNA Isolation kit (GE Healthcare, Little Chalfont, UK). Concentration and purity of RNA was measured using a ND-1000 Nanodrop Spectrophotometer (Nanodrop, Wilmington, DE, USA), comparative amounts of RNA were used for first-strand cDNA synthesized using SuperScript III (Invitrogen, Carlsbad, CA, USA) in accordance with the manufacturer's instructions. PCR was performed with specific primers (Table 3) using Go-Taq Green Master Mix (Promega Corp., Madison, WI, USA). PCR products were analysed on 2% agarose gels and visualized by ethidium bromide. qRT-PCR was performed with the same primers as PCR using Fast SYBR green chemistry (Applied Biosystems,

Table 3. Details of primers used

Gene name	Sequence (sense primer on top)	Accession #
<i>Gapdh</i>	GCCGATGCCCCATGTTTGTGA GGGTGGCAGTGATGGCATGGAC	NM_008084
<i>Pdgfra</i>	ATGACAGCAGGCAGGGCTTCAACG CGGCACAGGTCAACCAGATCGTTT	NM_011058
<i>Ano1</i>	TAACCCTGCCACCGTCTTCT ATGATCCTTGACAGCTTCTCTCC	NM_178642
<i>Kit</i>	CGCCTGCCGAAATGTATGACG GGTTCTCTGGGTTGGGGTTGC	NM_021099
<i>Myh11</i>	CCCAAGCAGCTAAAGGACAA AGGCACTTGCATTGTAGTCC	NM_013607

Foster City, CA, USA) on the 7900HT Real Time PCR System (Applied Biosystems).

Patch clamp experiments on identified cell phenotypes

Whole-cell patch clamp configuration was used to record currents from ICC that were identified by copGFP fluorescence and SMCs identified by their typical long spindle-shaped morphology. After sharp dissection of the mucosa, the smooth muscle layer was cut into small strips and equilibrated in Ca^{2+} -free Hanks' solution at 4°C (see above). Muscle strips were incubated in the same enzyme solution over a time period similar to that used for FACS sorting (see above). Strips were washed with Ca^{2+} -free Hanks' solution to remove the enzyme, and isolated cells were obtained by triturating the strips with smooth muscle growth medium (SMGM; Clonetics Corp., San Diego, CA, USA) using a glass pipette. The cell suspension was placed on to glass coverslips coated with murine collagen (2.5 mg mL^{-1} ; Becton-Dickinson) in 35 mm culture dishes. SMGM supplemented with 2 % antibiotic-anti-mycotic (Gibco, Grand island, NY, USA) and stem cell factor (5 ng mL^{-1} ; Sigma) was added 20 min after the cells were settled. The cells were used from 1 h after incubating at 37°C in a 95% O_2 –5% CO_2 incubator.

An Axopatch 200B patch clamp amplifier (Axon Instruments, Union City, CA, USA) and a 12-bit A/D converter (Digidata 1320A; Axon Instruments) were used to voltage clamp the cells at -80 mV. Micropipettes used for recordings had a resistance of 4–6 M Ω . All data were digitized and acquired using pClamp, version 10.0.0.61 (Axon Instruments) and analysed using Clampfit (Axon Instruments) and Prism (Graphpad Software Inc., San Diego, CA, USA) software. All experiments were performed using a calcium containing physiological salt solution (PSS) solution at 30°C with a CL-100 bath heater (Warner Instruments, Hamden, CT, USA).

Electrophysiological and contractile experiments on intact muscles

The fundus region of stomachs was pinned as a sheet to the base of a Sylgard silicone elastomer (Dow Corning Corp.) dish and the mucosa removed by sharp dissection. Strips of muscle (4–8 mm) were isolated from along the greater curvature and placed in a recording chamber with the submucosal surface of the circular muscle layer facing upward. Circular muscle cells were impaled with glass microelectrodes (resistances of 80–120 M Ω) and electrical activity was recorded as described previously (Burns *et al.* 1996). Briefly, transmembrane potentials were recorded with a high impedance amplifier (Axon Instruments) and stored on a PC running the data acquisition software AxoScope, version 10 (Axon Instruments). Images were prepared using Clampfit (Axon Instruments) and Corel Draw.

Parallel platinum electrodes were placed on either side of the muscle strips to elicit neural responses with square pulses of electrical field stimulation (EFS) (0.3 ms pulse duration, 1–20 Hz, train durations of 1 s, 10–15 V) delivered by a Grass S48 stimulator (Grass Instrument Company, Quincy, MA, USA). Isometric force measurements were performed using tissues (3–6 mm) prepared as described previously (Burns *et al.* 1996). Tissues were placed between two ring electrodes fixed at one end and mounted onto a Gould force transducer at the other end. EFS using similar parameters (1–30 s duration) as in electrophysiological experiments were used to elicit motor responses.

Solutions and drugs

The external solution for whole-cell recordings was a Ca²⁺-containing physiological salt solution consisting of (mM): 5 KCl, 135 NaCl, 2 CaCl₂, 10 glucose, 1.2 MgCl₂ and 10 Hepes adjusted to pH 7.4 with Tris. Cs⁺-rich internal solution contained (mM), 30 CsCl, 110 Caesium aspartate, 3 MgATP, 0.1 NaGTP, 0.1 EGTA, 0.01 CaCl₂, 10 Hepes and 10 glucose adjusted to pH 7.2 with Tris. For muscle studies, tissues were perfused with oxygenated KRB of the following composition (mM): 118.5 NaCl, 4.5 KCl, 1.2 MgCl₂, 23.8 NaHCO₃, 1.2 KH₂PO₄, 11.0 dextrose and 2.4 CaCl₂. The pH of the KRB was 7.3–7.4 when bubbled with 97% O₂–3% CO₂ at 37 \pm 0.5°C. Muscles were equilibrated for at least 1 h before the experiments were initiated.

Carbamylcholine (CCh), lanthanum, L-N^G-Nitroarginine (L-NNA), neostigmine, atropine, 5-nitro-2-(3-phenylpropylamino)benzoic acid (NPPB), benzbro-morone and tamoxifen were obtained from Sigma. 2-(5-ethyl-4-hydroxy-6-methylpyrimidin-2-ylthio)-N-(4-(4-methoxyphenyl)thiazol-2-yl)acetamide (T16A_{inh}-A01) was purchased from Calbiochem (Darmstadt, Germany). CCh and lanthanum (La³⁺) were dissolved

in water and NPPB and T16A_{inh}-A01 were dissolved in DMSO. Final concentrations of DMSO were less than 0.1%. Tamoxifen was dissolved in safflower oil. For some muscle electrophysiological experiments, nifedipine (Sigma) was dissolved in ethanol at a stock concentration of 100 μ M before being added to the perfusion solution at a final concentration of 1 μ M to inhibit contractile activity.

Statistical analysis

For morphological studies, the numbers of ICC-IM were counted in six random fields of view of fundus muscles from *Ano1*^{+/+} and *Ano1*^{-/-} mutants taken at 40 \times magnification. The number of ICC-IM in each muscle layer was calculated as the number of cells crossing a 100 μ m transactional line drawn perpendicular to the axis of the circular or longitudinal muscle layer.

For analysis of molecular studies, gene transcript expression was compared between eGFP⁺-SMCs, CopGFP⁺-ICC and eGFP⁺-PDGFR α ⁺, and each cell type was also compared with total cell population of fundus tunica muscularis. Regression analysis of the mean values of three multiplex qPCRs for the log₁₀ diluted cDNA was used to generate standard curves. Unknown amounts of mRNA were plotted relative to the standard curve for each set of primers and graphically plotted using Excel (Microsoft Corp., Redmond, WA, USA). Primer efficiencies of 90–110% were only accepted for analysis. This gave transcriptional quantification of each gene relative to the endogenous *Gapdh* standard after log transformation of the corresponding raw data. In pilot studies, *Gapdh* was tested on all three cell types used in the present study and represents an appropriate control for qPCR analyses. Normalized values and SDs were calculated in differences of relative gene expression from four dilutions of technical duplicates from each animal. The data are shown as the mean \pm SD of triplicate samples ($n = 3$). For the fold change of genes with, $P < 0.05$ was considered statistically significant. An unpaired Student's *t* test was used to determine *P* values in the parametric analysis.

Several electrical parameters were analysed: (i) resting membrane potential (RMP); (ii) amplitude of EJPs; (iii) half-maximal duration of EJPs; (iv) unitary potentials; and (v) for isometric force measurements, area under the trace. Images were made from digitized data using Corel Draw X4. Nerve evoked responses were compared between age-matched *Ano1*^{+/+} and *Ano1*^{-/-} siblings or tamoxifen treated *c-Kit*^{CreERT21Ejb/+}; *Ano1*^{f/+} control and *c-Kit*^{CreERT21Ejb/+}; *Ano1*^{fff} mutants.

Data are expressed as the means \pm SEM. Differences between the reported means of mouse groups were evaluated using an unpaired Student's *t* test. $P < 0.05$ was considered as a statistically significant difference.

Differences between the means of three or more measured parameters were evaluated using repeated measures ANOVA where appropriate in conjunction with the Dunnett's multiple comparison test. Again, $P < 0.05$ was considered statistically significant. Statistical tests were performed using Prism, version 5.03 (GraphPad Software Inc.). The reported n values refer to the number of animals used for each experimental protocol.

Results

Ano1-like immunoreactivity in ICC-IM and close apposition to cholinergic nerves

Double-labelling immunohistochemistry using antibodies against Kit and Ano1 showed that spindle-shaped Kit⁺ ICC-IM within the circular and longitudinal muscle layers of the gastric fundus were immunopositive for Ano1 (Ano1⁺) (Fig. 1A–C). Kit and Ano1 labelling was also performed on gastric fundus muscles from P3–P5 animals to test whether a similar relationship existed in younger animals. We used animals in this age range during the course of the present study because most global knockouts of *Ano1* (*Ano1*^{-/-} mice) die within 1 week after birth (Rock *et al.* 2008). Similar to adults, fundus ICC-IM were Ano1⁺ in P3–P5 animals (Fig. 1D–I).

ICC-IM were spindle shaped and closely associated with varicose motor nerve fibres, as shown by labelling with the pan neuronal marker protein-gene product 9.5, as reported previously (Burns *et al.* 1996; Ward

et al. 2000). Ano1 expression was not resolved in Kit⁻ cells. Double-labelling studies with antibodies against vesicular acetylcholine transporter (VACHT) and Kit were performed to highlight specifically the morphological relationship between cholinergic nerve fibres and ICC-IM. Close contacts between VACHT immunopositive (VACHT⁺) varicose nerve fibres and Kit⁺ ICC-IM were observed for $>250 \mu\text{m}$ along the surfaces of ICC-IM (Fig. 2A–F). vAChT and Kit immunohistochemistry was also performed on fundus muscles from P3–P5 mice, and similar close alignments were observed between VACHT⁺ nerve fibres and ICC-IM in these young animals (Fig. 2G–L).

CCh activates inward currents in ICC and SMCs of murine fundus

Cholinergic neurotransmission in GI muscles, mediated by muscarinic receptors, generates depolarization of post-junctional cells known as EJPs (Bennett, 1966; Ward *et al.* 2000; Matsuyama *et al.* 2013). We investigated the conductances activated by muscarinic stimulation in isolated and identified ICC-IM and SMCs from the murine fundus using the whole-cell patch clamp technique. A Cs⁺-rich pipette solution with $E_{\text{Cl}} = -40 \text{ mV}$ was used to study the properties of CCh-induced inward currents in ICC-IM and SMCs. Cell capacitance averaged $5.5 \pm 0.4 \text{ pF}$ ($n = 28$) for ICC and $25.0 \pm 1.6 \text{ pF}$ ($n = 21$) for SMCs. Holding currents were $-7.0 \pm 1.1 \text{ pA pF}^{-1}$ and $-0.5 \pm 0.1 \text{ pA pF}^{-1}$ at -80 mV for ICC and

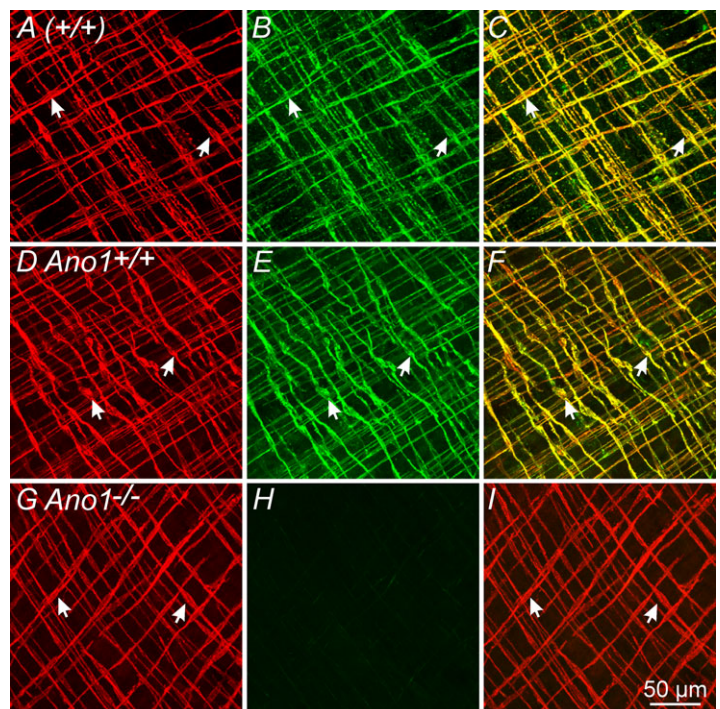


Figure 1. Double-labelling immunohistochemistry reveals Kit and Ano1 expression in ICC-IM of the gastric fundus of adult and neonatal mice

A–C, confocal reconstructions demonstrate Kit⁺ ICC-IM (A, arrows, red) and Ano1⁺ localization (B, arrows, green) in the gastric fundus of an adult (+/+) mouse. C, merged image showing cellular co-localization of Kit and Ano1 (arrows, yellow). D–F, in gastric fundus of P5 *Ano1*^{+/+} animals, Ano1 is also expressed in ICC-IM. D, Kit⁺ ICC-IM (arrows, red); E, Ano1⁺ ICC-IM (arrows, green). F, merged image of (D) and (E) showing cellular co-localization of Kit and Ano1 (arrows, yellow). G–I, absence of Ano1 immunoreactivity in *Ano1*^{-/-} mutants and confirmation of specificity of Ano1 antibody used. G, Kit⁺ ICC-IM were readily identified in P5 *Ano1*^{-/-} mutant animals (red, arrows) but Ano1 immunoreactivity was not detectible (H). I, merged image of (G) and (H) revealing Kit⁺ ICC-IM but absence of Ano1 in ICC-IM of *Ano1*^{-/-} mutants. Scale bar = 50 μm .

SMCs, respectively. CCh ($10 \mu\text{M}$), applied using a rapid perfusion Valvelink 8.2 digital solenoid valve controller (Automate Scientific, Inc., Berkley, CA, USA), evoked large amplitude inward currents in ICC-IM, averaging $-213.2 \pm 32.5 \text{ pA pF}^{-1}$ at -80 mV ($n = 8$; $P < 0.01$) (Fig. 3A–C). These large currents were transient in nature, most probably a result of the rapid release and unloading of calcium from intracellular stores as previously shown (Pacaud & Bolton, 1991*b*). Small amplitude, noisy inward currents were evoked in SMCs under the same conditions averaging $-1.2 \pm 0.1 \text{ pA}$ ($n = 7$; $P < 0.01$) (Fig. 3D–F). Atropine ($1 \mu\text{M}$) inhibited the responses to CCh in ICC (Fig. 3G and I) and SMCs (Fig. 3H and J).

Nature of the conductance activated in ICC-IM and SMCs

A CaCC mediated by Ano1 is expressed by ICC but not resolved in SMCs in GI muscles (Gomez-Pinilla *et al.* 2009; Hwang *et al.* 2009; Zhu *et al.* 2009 Rhee *et al.* 2011; Blair *et al.* 2012). EJPs in the fundus in response to cholinergic neurotransmission may be mediated by activation of CaCC. Spontaneous transient inward currents (STICs)

were observed in many ICC held at -80 mV . STICs reversed between -30 and -20 mV (before correction of the junction potential calculated to be 14.6 mV in our experiments) using a Cs^+ -rich pipette solution with $E_{\text{Cl}} = -40 \text{ mV}$ (Fig. 4A and B). NPPB ($10 \mu\text{M}$), decreased holding currents from $-13.9 \pm 2.8 \text{ pA pF}^{-1}$ to $-2.5 \pm 0.7 \text{ pA pF}^{-1}$ and inhibited STICs ($P < 0.05$; $n = 5$) (Fig. 4C and D), suggesting that that STICs and part of the holding current were a result of CaCC. NPPB added 5 min before CCh application blocked the inward currents evoked by CCh ($-5.0 \pm 1.6 \text{ pA pF}^{-1}$; $n = 5$; $P > 0.05$ when comparing NPPB and NPPB after CCh addition; $n = 5$) (Fig. 4E–G).

Two second generation Ano1 blockers, benz-bromarone (Huang *et al.* 2012) and T16A_{inh}-A01 (Namkung *et al.* 2011), blocked STICs and currents evoked in ICC-IM by CCh. Benzbromarone ($1 \mu\text{M}$) reduced holding currents from $-19.1 \pm 3.7 \text{ pA pF}^{-1}$ to $-2.7 \pm 0.4 \text{ pA pF}^{-1}$ and STICs in ICC-IM. Inward currents evoked by CCh were reduced by benzbromarone ($1 \mu\text{M}$; $P < 0.01$ compared to control; $n = 5$) (Fig. 5A–C). T16A_{inh}-A01 reduced holding currents from $-13.3 \pm 2.2 \text{ pA pF}^{-1}$ to $-3.4 \pm 0.8 \text{ pA pF}^{-1}$ at $10 \mu\text{M}$ and from $-9.3 \pm 2.9 \text{ pA pF}^{-1}$ to $-2.4 \pm 0.6 \text{ pA pF}^{-1}$ at

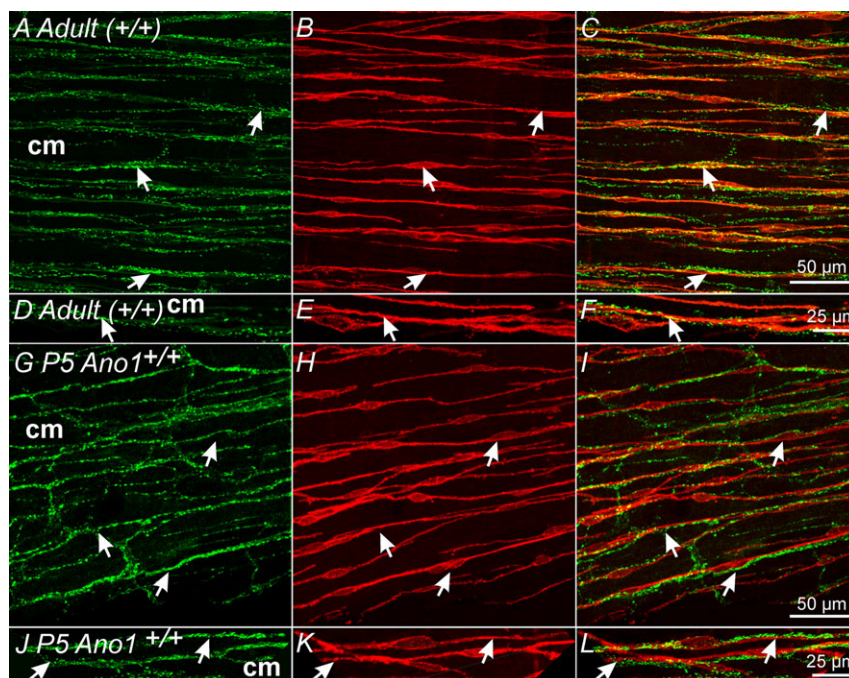


Figure 2. Ano1⁺ ICC-IM are closely apposed to vAChT⁺ nerve fibres in the gastric fundus

A–C, varicose vAChT⁺ nerve fibres (A, arrows, green) and Ano1⁺ ICC-IM (B, arrows, red) within the circular layer (cm) of adult (+/+) fundus muscles. C, merged image showing the close apposition between vAChT⁺ nerve fibres and Ano1⁺ ICC-IM (arrows). D–F, higher power images of the relationship between vAChT⁺ nerves and Ano1⁺ ICC-IM. vAChT⁺ nerves were closely apposed to Ano1⁺ ICC-IM for $>250 \mu\text{m}$. G–I, gastric fundus muscles of P5 *Ano1*^{+/+} animals also display a similar close morphological relationship between vAChT⁺ nerves and Ano1⁺ ICC-IM as seen in adult animals. G, vAChT⁺ nerve fibres (arrows, green) and Ano1⁺ ICC-IM (H, arrows, red) in the circular layer (cm). I, similar to adult tissues, vAChT⁺ nerves were closely apposed to Ano1⁺ ICC-IM for $>250 \mu\text{m}$. J–L, at higher magnification, the close apposition between vAChT⁺ nerve fibres and Ano1⁺ ICC-IM can be readily observed. Scale bars for each series of confocal reconstructions are shown in (C), (F), (I) and (L).

30 μM , respectively ($P < 0.05$ for 10 and 30 μM ; $n = 5$ for each concentration) (Fig. 5D–H). Inward currents evoked by CCh were reduced by 10 μM T16A_{inh}-A01 (to -47.0 ± 6.8 pA pF⁻¹; $P < 0.01$ compared to control) and blocked by 30 μM T16A_{inh}-A01 (to -3.6 ± 1.2 pA pF⁻¹) ($n = 5$ for each concentration) (Fig. 5D–H).

Although Ano1 was not resolved in SMCs of the fundus (Figs 1, 8 and 9), experiments aiming to examine the effects of the Ano1 inhibitors were also performed on isolated SMCs. At -80 mV, SMCs generated small holding currents and T16A_{inh}-A01 (10 and 30 μM) did not affect these currents. As described above, CCh activated small amplitude noisy inward currents in SMCs and T16A_{inh}-A01 did not affect these responses

(-1.6 ± 0.1 pA pF⁻¹ at 10 μM and -1.6 ± 0.3 pA pF⁻¹ at 30 μM , respectively; $n = 5$ for each concentration) (Fig. 5I–K).

We also tested whether the inward current evoked by CCh in ICC-IM might be mediated partially by a NSCC by testing the effects of La³⁺ pretreatment. La³⁺ (10 μM) tended to reduce holding currents slightly, although this effect did not reach statistical significance. La³⁺ also had little effect on STICs in ICC-IM. In the presence of La³⁺, CCh (10 μM) evoked large amplitude inward currents (i.e. to -176.3 ± 40.5 pA pF⁻¹; $P < 0.01$; $n = 5$) (Fig. 6A–C). These results, in accordance with complete block of responses by CaCC blockers, suggest that NSCC does not contribute significantly to CCh responses in

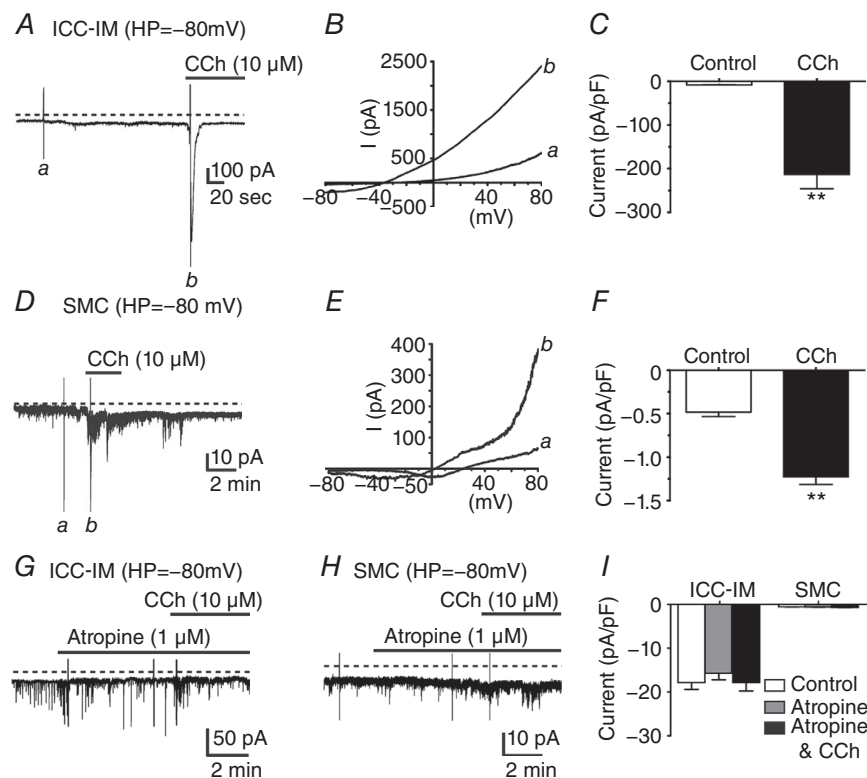


Figure 3. Carbachol activates a large inward conductance in ICC-IM and a small noisy conductance in fundus SMCs

A, at a holding potential (HP) of -80 mV with a Cs⁺-rich pipette solution and $E_{\text{Cl}^-} = -40$ mV, ICC-IM displayed a sustained inward conductance. Addition of carbachol (CCh, 10 μM) activated a large amplitude transient inward current in ICC-IM. B, voltage ramp protocols reveal the current activated by CCh. Current in response to voltage ramp from -80 to $+80$ mV before (a) and after CCh (b), at the time points indicated in (A). After CCh, voltage ramps reversed at around -40 mV. C, summary of the normalized current density activated by CCh. CCh evoked inward current averaging -213.2 ± 32.5 pA pF⁻¹ in ICC-IM ($n = 8$; $**P < 0.01$). D–F, in SMCs, CCh (10 μM) activated a small noisy inward conductance in fundus SMCs. D, under conditions similar to those performed on ICC-IM (HP = -80 mV), SMCs had smaller holding currents (Da) and addition of CCh (10 μM) (Db) activated small noisy currents. E, voltage ramp protocols performed before (a) and after CCh (b), at the time points indicated in (D). Ramps in the presence of CCh reversed at ~ 0 mV. F, normalized current density activated by CCh in SMCs averaged -1.2 ± 0.1 pA pF⁻¹ ($n = 7$; $**P < 0.01$). G, atropine inhibited inward currents activated by CCh in ICC-IM but not STICs, H, atropine also inhibited activation of noisy currents in SMCs. I, summary showing that atropine blocked CCh responses in both ICC-IM and SMCs ($n = 8$ for ICC-IM and $n = 7$ for SMCs; $P > 0.05$ for both cell types).

ICC-IM of the fundus. The inward currents induced by CCh in SMCs were probably the result of activation of NSCC, as reported previously (Dwyer *et al.* 2011). Therefore, we tested the effects of lanthanum (La^{3+}) on the CCh-induced currents in SMCs (Fig. 6D–F). Ramp protocols applied in the presence of CCh revealed a reversal potential of 0 mV ($E_{\text{Cl}^-} = -40$ mV) (Fig. 6E). La^{3+} ($10 \mu\text{M}$), added 10 min before application of CCh ($10 \mu\text{M}$), reduced inward currents evoked by CCh significantly (to -0.7 ± 0.1 pA pF $^{-1}$ in the presence of La^{3+} and -0.9 ± 0.2 pA pF $^{-1}$ in the presence of La^{3+} after CCh addition; $P > 0.05$ when comparing La^{3+} with La^{3+} after CCh addition; $n = 5$) (Fig. 6F). These data suggest that CCh activates a NSCC in fundus SMCs.

Cholinergic responses in intact muscles require Ano1

CCh activates different conductances in ICC-IM and SMCs, and so the suppression of currents carried by Ano1 channels may provide evidence of whether ICC are the cells primarily responsible for post-junctional electrical responses to cholinergic neurotransmission. We measured electrophysiological responses of intact fundus muscles to electrical field stimulation (EFS) of intrinsic neurons in mice with global deactivation of *Ano1* (known formerly as *Tmem16a*, so that the strain name of these mice is *Tmem16a*^(tm1Bdh)(*tm1Bdh*); Rock *et al.* 2008). In this part of the study, fundus muscles were harvested from P5 mice as a result of the short life span of these animals. Post-junctional responses to

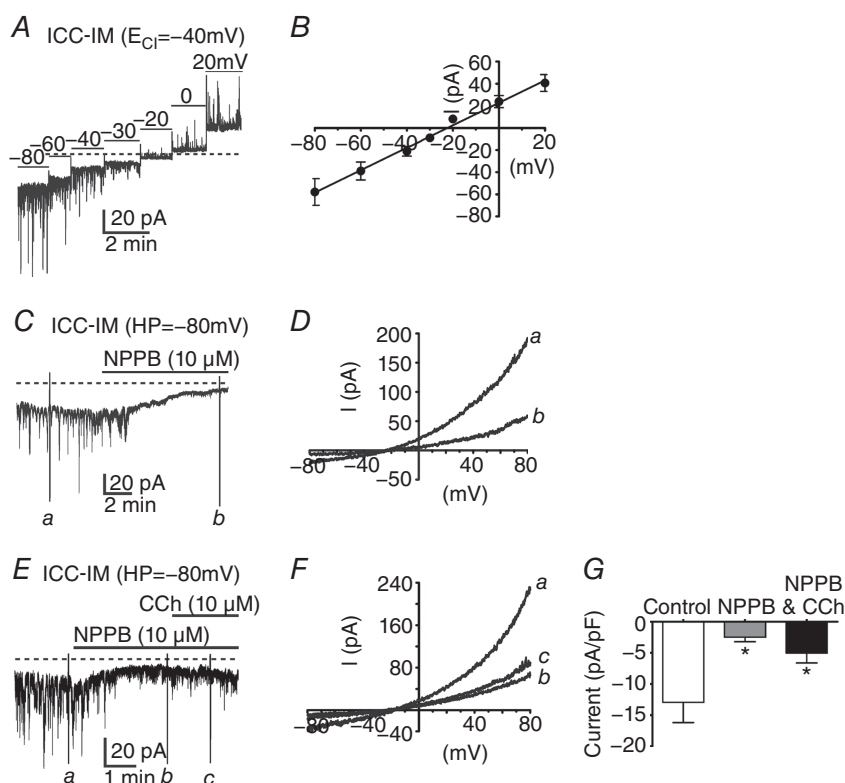


Figure 4. The CaCC blocker NPPB inhibited CCh activation of inward currents in ICC-IM

A, spontaneous transient inward currents (STICs) in ICC-IM at voltage steps from -80 to $+20$ mV. Large STICs were observed in ICC-IM held at potentials between -80 mV and -40 mV. B, STICs reversed at potentials between -30 and -20 mV (before correction of junction potential; calculated junction potential = 14.6 mV) using a Cs^+ -rich pipette solution with $E_{\text{Cl}^-} = -40$ mV. C and D, CaCC channel blocker NPPB ($10 \mu\text{M}$) blocked the sustained inward current and STICs, suggesting that these events were a result of CaCC. NPPB decreased holding currents from -13.9 ± 2.8 pA pF $^{-1}$ to -2.5 ± 0.7 pA pF $^{-1}$ ($P < 0.05$; $n = 5$). D, currents recorded in response to voltage ramps under control conditions (a) were reduced significantly by NPPB (b). Voltage ramps were applied at the time points indicated in (C). E–G, NPPB and CCh-induced inward currents in ICC-IM. E, NPPB ($10 \mu\text{M}$) reduced STICs and holding currents in ICC-IM. CCh, in the presence of NPPB, added 5 min before CCh application, failed to activate inward current in ICC-IM. F, voltage ramp protocols performed before (a) and after addition of NPPB (b) and after addition of CCh ($10 \mu\text{M}$), at the time points indicated in (E). Control voltage ramps were reduced by NPPB and CCh failed to activate inward current in response to voltage ramps in the presence of NPPB. G, summary of currents activated in response to voltage ramps under control conditions (white bar) and reduction in currents after addition of NPPB ($10 \mu\text{M}$; grey bar) and CCh ($10 \mu\text{M}$) in the continued presence of NPPB (black bar; $n = 5$; $*P < 0.05$, one-way ANOVA).

cholinergic neurotransmission in muscles of *Ano*^{+/+} and *Ano1*^{-/-} animals were compared. EFS was applied and responses were recorded: (i) under control conditions with no drugs present; (ii) in the presence of the nitric oxide synthase inhibitor L-NNA (100 μ M) to unmask EJPs; (iii) in the continued presence of L-NNA and after addition of an acetylcholinesterase (AChE) inhibitor,

neostigmine (1 μ M) to determine whether ACh activates post-junctional receptors not normally stimulated when ACh is being metabolized; and (iv) in the presence of L-NNA, neostigmine and atropine (1 μ M) to confirm that EJPs were evoked via muscarinic receptors.

Membrane potentials recorded from circular muscle cells of *Ano1*^{+/+} muscles averaged -45.3 ± 1.4 mV

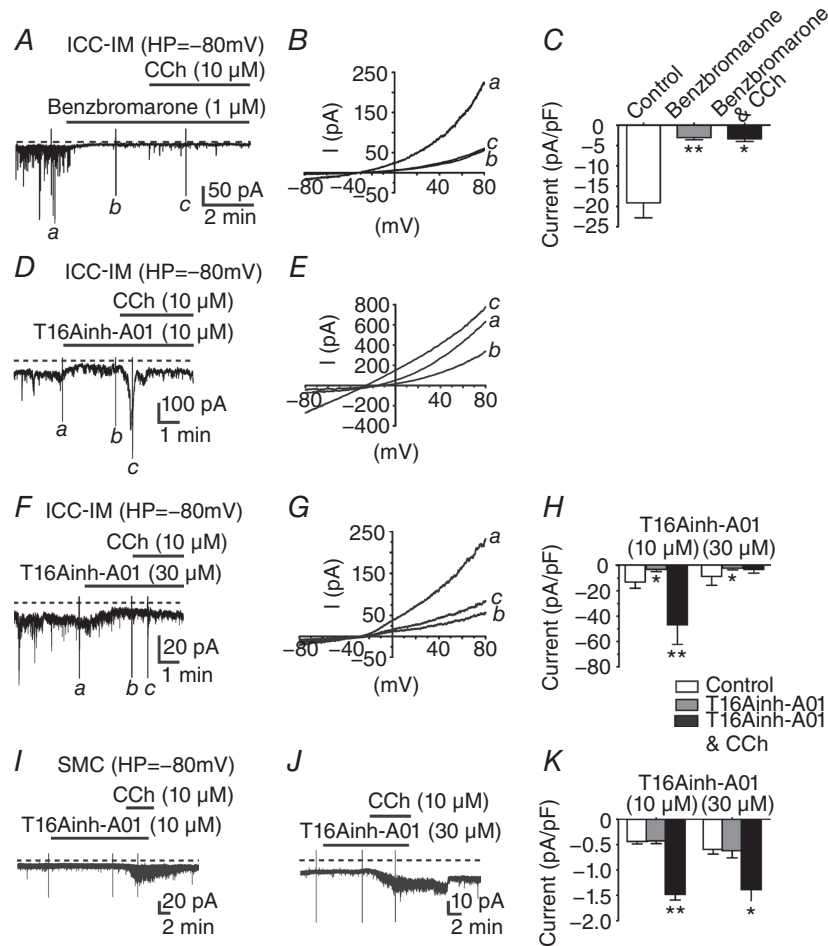


Figure 5. Second generation *Ano1* inhibitors blocked STICs and CCh induced currents in ICC-IM but not SMCs

A–C, benzbromarone (1 μ M) inhibited sustained inward current and STICs in ICC-IM. *B*, inward currents in response to voltage ramp protocols applied under control conditions (*a*) were reduced significantly in benzabromarone (*b*) and in the presence of CCh (10 μ M) (*c*). Time points for (*a*) to (*c*), where ramps were applied are shown in *A*. *C*, summarized responses of normalized current densities applied under control conditions, in benzbromarone and in benzbromarone and CCh ($n = 5$). *D–H*, effects of T16A_{inh}-A01 (10–30 μ M) on sustained and CCh-induced inward currents in ICC-IM. *D* and *E*, T16A_{inh}-A01 (10 μ M) reduced sustained inward current and CCh (10 μ M) induced current. Voltage ramp protocols applied at the time points (*a*) to (*c*) in (*D*) under control conditions (*a*) were reduced by T16A_{inh}-A01 (*b*) but increased after CCh (*c*). *F* and *G*, at higher concentrations, T16A_{inh}-A01 (30 μ M) reduced sustained current and CCh evoked inward currents. Voltage ramp protocols in (*G*) were applied at the time points (*a*), (*b*) and (*c*) in (*F*). *H*, summary of CCh evoked responses (pA pF⁻¹) in T16A_{inh}-A01 (10 and 30 μ M). T16A_{inh}-A01 (10 and 30 μ M) inhibited sustained inward currents but 30 μ M was necessary to inhibit CCh evoked inward currents. *I–K*, effects of T16A_{inh}-A01 (10 and 30 μ M) on CCh evoked currents in SMCs. *I* and *J*, T16A_{inh}-A01 (10 and 30 μ M) did not inhibit noisy sustained inward currents or CCh evoked currents in SMCs. *K*, summary of normalized current density under control conditions (white bar), in T16A_{inh}-A01 (grey bar) and CCh in the continued presence of T16A_{inh}-A01 (black bar). CCh still evoked responses in SMCs in T16A_{inh}-A01. Summarized data in (*C*), (*H*) and (*K*), * $P < 0.05$; ** $P < 0.01$ one-way ANOVA.

($n = 8$). Fundus muscles in the mouse do not display slow waves (Burns *et al.* 1996) but, instead, generate small amplitude, noisy oscillations, known as spontaneous transient depolarizations (STDs) or unitary potentials (Burns *et al.* 1996; Edwards *et al.* 1999; Van Helden *et al.* 2000; Beckett *et al.* 2004). Under control conditions, EFS (0.3 ms pulses, 1–20 Hz, 1 s) evoked a biphasic response consisting of an EJP that averaged 4.1 ± 2.2 mV in amplitude and 179 ± 52 ms (half-maximal amplitude duration; 1 Hz; 0.3 ms pulse duration) followed by a more sustained hyperpolarization or inhibitory junction potential (IJP) (3.5 ± 1.1 mV; $n = 8$). EJPs and IJPs were frequency-dependent and increased in amplitude and duration as the stimulus frequency increased (e.g. EJP = 5.2 ± 2.8 mV in amplitude and 229 ± 66 ms in half-maximal amplitude duration; IJP = 7.3 ± 1.3 mV in amplitude at 10 Hz stimulation) (Fig. 7A).

RMP was unchanged by L-NNA ($100 \mu\text{M}$; -46.1 ± 1.9 mV; $P > 0.05$ vs. control) but EJPs increased to 8.2 ± 2.6 mV in amplitude and 304 ± 43 ms (half-maximal amplitude duration) at 1 Hz and 10.4 ± 2.8 mV in amplitude and 860 ± 86 ms at 10 Hz after addition of L-NNA (Fig. 7B). In the continued presence of L-NNA, addition of neostigmine caused membrane depolarization to -40.2 ± 1.9 mV ($P < 0.05$ vs. L-NNA and control) and EFS evoked a biphasic response consisting of a fast EJP (i.e. 10.4 ± 1.5 mV at 1 Hz and 12.4 ± 0.9 mV at 5 Hz) and a secondary, slower and longer-lasting depolarization that often merged with the fast EJP. The slow depolarization averaged 6.4 ± 1.0 mV and the half-maximal amplitude duration of 5586 ± 809 ms at 1 Hz and 14 ± 2.7 mV and 9161 ± 911 ms at 5 Hz (Fig. 7C). The fast and slow components of the responses to EFS in the presence of neostigmine were inhibited by

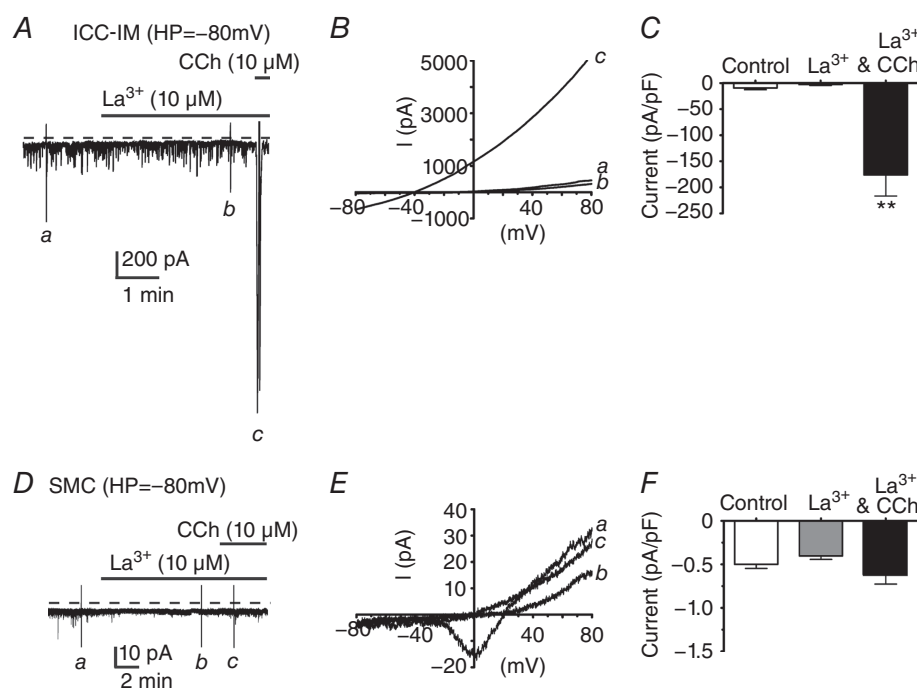


Figure 6. The non-selective cation channel inhibitor lanthanum did not block CCh activated currents in ICC-IM but blocked CCh activated currents in SMCs

A, lanthanum (La^{3+} , $10 \mu\text{M}$) had little effect on holding current and on STICs in ICC-IM. CCh ($10 \mu\text{M}$) in the presence of La^{3+} , activated a large transient inward current. B, currents activated in response to voltage ramps applied at the time points (a), (b) and (c) indicated in (A). In the presence of La^{3+} , CCh activated large currents in ICC-IM. C, summary of normalized current densities (pA pF^{-1}) under control conditions (white bar), in La^{3+} ($10 \mu\text{M}$; grey bar) and CCh ($10 \mu\text{M}$) in the continued presence of La^{3+} (black bar). CCh activated currents in La^{3+} averaged $-176.3 \pm 40.5 \text{ pA pF}^{-1}$ in ICC-IM ($n = 5$; $P < 0.01$). D–F, effects of La^{3+} on the CCh-induced currents in SMCs. D, La^{3+} ($10 \mu\text{M}$) reduced small noisy currents recorded from SMCs and, in the continued presence of La^{3+} , CCh did not increase noisy current. E, currents activated in response to voltage ramp protocols applied in the presence of CCh revealed a reversal potential of 0 mV ($E_{\text{Cl}^-} = -40 \text{ mV}$). La^{3+} ($10 \mu\text{M}$), added 10 min before application of CCh ($10 \mu\text{M}$), reduced inward currents evoked by CCh. Voltage ramps applied at the time points (a), (b) and (c) indicated in (D). In the presence of La^{3+} , CCh did not significantly increase currents in SMCs. F, summary of normalized current densities (pA pF^{-1}) under control conditions (white bar), in La^{3+} ($10 \mu\text{M}$; grey bar) and CCh ($10 \mu\text{M}$) in the continued presence of La^{3+} (black bar). CCh did not cause a significant increase in currents in SMCs in the presence of La^{3+} ($-0.7 \pm 0.1 \text{ pA pF}^{-1}$ in the presence of La^{3+} and $-0.9 \pm 0.2 \text{ pA pF}^{-1}$ in the presence of La^{3+} after CCh addition; $P > 0.05$ when comparing La^{3+} with La^{3+} after CCh addition; $n = 5$).

atropine (Fig. 7D), confirming that both were mediated by muscarinic receptors.

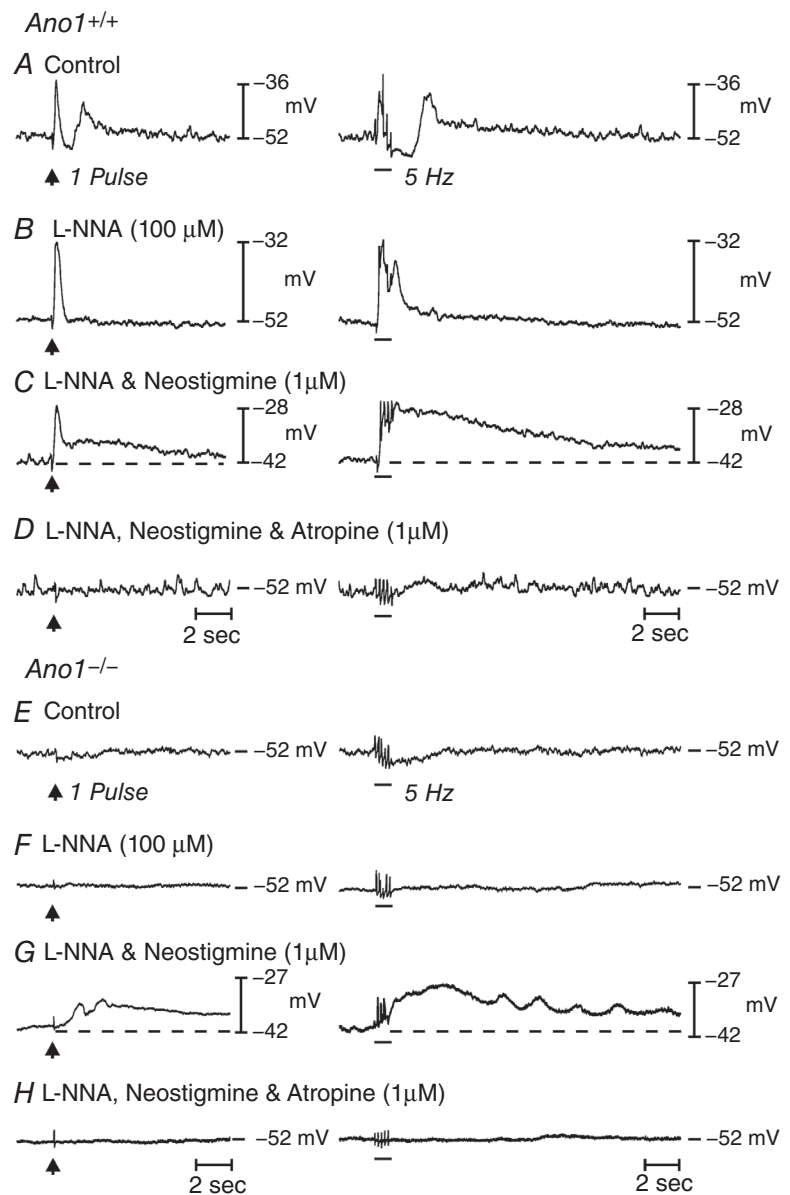
Cells of fundus muscles from *Ano1*^{-/-} mice had resting potentials averaging -45.3 ± 1.5 mV ($n = 15$; $P > 0.05$ compared to *Ano1*^{+/+}) and the small oscillations in membrane potential (STDs or unitary potentials) (Burns *et al.* 1996; Edwards *et al.* 1999; Van Helden *et al.* 2000; Beckett *et al.* 2004) observed after impalement of cells in *Ano1*^{+/+} muscles were greatly attenuated or not resolvable in *Ano1*^{-/-} muscles. EFS (1–20 Hz) failed to elicit EJPs before or after L-NNA ($P > 0.05$ vs. control) (Fig. 7E and F). However, neostigmine (in the continued presence of L-NNA) continued to cause depolarization (to -39.0 ± 1.3 mV; $P < 0.001$) and EFS caused slowly developing depolarization responses,

averaging 2.6 ± 0.6 mV in amplitude and 3410 ± 882 ms in duration at half-maximal amplitude at 1 Hz and 6.8 ± 1.5 mV in amplitude and 10500 ± 1196 ms in duration at half-maximal amplitude at 5 Hz (Fig. 7G). Responses elicited after neostigmine were blocked by atropine (Fig. 7H). Fully developed myenteric ganglia (not shown) and innervation of circular muscles by vAChT⁺ (cholinergic) motor neurons were observed in P5 mice (Fig. 2), suggesting that reduced cholinergic neurotransmission in these young animals was not the result of a paucity of motor neurons. Furthermore, there was no loss of vAChT⁺ neurons in *Ano1*^{-/-} mice compared to *Ano1*^{+/+} controls (Fig. 2).

Ano1 is reported to be necessary for the development or proliferation of ICC (Stanich *et al.* 2011). We investigated

Figure 7. Nerve evoked post junctional responses in P5 *Ano1*^{+/+} and *Ano1*^{-/-} mutant fundus muscles in response to EFS

A, neural responses in *Ano1*^{+/+} fundus muscles under control conditions in response to EFS, 1 Hz (delivered at arrow, left) and 5 Hz (horizontal bar, right) respectively ($n = 8$). EFS evoked a frequency-dependent biphasic motor response consisting of an initial fast transient EJP followed by a more sustained IJP that was often followed by a secondary depolarization in membrane potential before it returned to pre-stimulus levels. B, in the presence of L-NNA (100 μ M), the EFS evoked IJP was abolished and the EJP increased in amplitude. C, in the continued presence of L-NNA, neostigmine (1 μ M) depolarized membrane potential, evoked an EJP and revealed a slower developing and more sustained depolarization in membrane potential (dashed lines) to EFS. D, atropine (1 μ M) abolished both the initial and sustained depolarization at all EFS frequencies examined. E, in *Ano1*^{-/-} mutants, EFS evoked little or no post-junctional responses to EFS under control conditions at 1 Hz and a small hyperpolarization at 5 Hz ($n = 15$). F, L-NNA (100 μ M) produced little change to EFS at 1 pulse but attenuated the slight hyperpolarization in membrane potential at 5 Hz. G, in the continued presence of L-NNA, neostigmine (1 μ M) caused membrane depolarization and produced a slowly developing and sustained depolarization response to EFS, as in *Ano1*^{+/+} animals. H, atropine repolarized membrane potential and blocked the nerve evoked depolarization observed in the presence of neostigmine at all frequencies tested. Note also the difference in basal electrical activity between *Ano1*^{+/+} and *Ano1*^{-/-} mutants.



whether ICC were reduced in *Ano1*^{-/-} mutants, which could also explain the compromised post-junctional responses to cholinergic neurotransmission (Burns *et al.* 1996; Ward *et al.* 2000). Densities of ICC-IM in the fundus of *Ano1*^{+/+} and *Ano1*^{-/-} mice were compared using Kit immunohistochemistry. P5 *Ano1*^{+/+} mice had an average of 9.8 ± 0.4 ICC-IM and *Ano1*^{-/-} mutants had an average of 11.3 ± 0.5 ICC-IM in the circular layer and 5.4 ± 0.5 ICC-IM and 7.2 ± 0.2 ICC-IM in the longitudinal layers of *Ano1*^{+/+} and *Ano1*^{-/-} mutants per 100 μm cross-sectional transection line. Differences in ICC-IM were not significant in the circular and longitudinal muscle layers of *Ano1*^{-/-} mice in comparison to *Ano1*^{+/+} age-matched controls ($P > 0.1$; when comparing the number of ICC in *Ano1*^{+/+} and *Ano1*^{-/-} circular or

longitudinal muscle layers, respectively ($n = 5$ for each group) (Fig. 8).

The lack of cholinergic neurotransmission that we observed in P5 global *Ano1*^{-/-} mice might conceivably result from unknown developmental factors. Therefore, we also performed experiments on mice with conditional knockdowns of *Ano1*, using tamoxifen treated *Kit*^{CreERT2/+}; *Ano1*^{tm1jrr/+} control (*iAno1*^{+/-}) and *Kit*^{CreERT2/+}; *Ano1*^{tm1jrr/-} (*iAno1*^{-/-}) mice. The efficiency of the inducible Cre-recombinase was examined in *Kit*^{CreERT2/+}; *Ano1*^{tm1jrr/+}; *Rosa*^{mtmg} (*iAno1*^{+/-}; *Rosa*) and *Kit*^{CreERT2/+}; *Ano1*^{tm1jrr/-}; *Rosa*^{mtmg} (*iAno1*^{-/-}; *Rosa*) mice. eGFP was expressed in ICC-IM in both *iAno1*^{+/-}; *Rosa* and *iAno1*^{-/-}; *Rosa* mice after tamoxifen treatment, supporting Cre-recombination (Fig. 9A and B). It should be noted that Cre-recombinase was also induced in small round cells in the gastric fundus by tamoxifen treatment (Fig. 9C). These cells are probably mast cells that are also *Kit*⁺. After tamoxifen, *Ano1* expression was reduced significantly in the gastric fundus of *iAno1*^{-/-} and *iAno1*^{-/-}; *Rosa* mice, as shown by qPCR and *Ano1* immunohistochemistry, compared to tamoxifen treated *iAno1*^{+/-} and *iAno1*^{+/-}; *Rosa* mice (Fig. 9D–I). Gastric fundus muscles of *iAno1*^{-/-} mice showed a 4.3-fold reduction (0.017 ± 0.001) in *Ano1* transcripts compared to age-matched *iAno1*^{+/-} siblings (0.073 ± 0.003 ; $P < 0.001$; $n = 4$ animals for both). There was no significant difference in *Ano1* transcript expression between tamoxifen treated *iAno1*^{+/-} mice and (+/+) mice (0.065 ± 0.002 ; $P > 0.05$; $n = 4$ for both).

Although ICC-IM were not reduced in global *Ano1*^{-/-} mice (Fig. 8) or in tamoxifen treated *iAno1*^{-/-} or *iAno1*^{-/-}; *Rosa* mice (Fig. 9), we found a significant reduction (–4.6-fold) in *Kit* transcripts (i.e. from 0.078 ± 0.004 in *iAno1*^{+/-} mice to 0.017 ± 0.001 in *iAno1*^{-/-} mice ($P < 0.001$; $n = 4$). Again, there was no significant difference in *Kit* transcripts between tamoxifen treated *iAno1*^{+/-} mice and (+/+) mice (0.085 ± 0.001 ; $P > 0.05$).

Pdgfra transcripts, a biomarker for PDGFR α ⁺ cells (Iino *et al.* 2009; Kurahashi *et al.* 2011), were changed significantly: 0.11 ± 0.006 in (+/+) and 0.086 ± 0.001 in *iAno1*^{+/-} compared to 0.048 ± 0.001 in *iAno1*^{-/-} fundus muscles ($P < 0.05$ when comparing *iAno1*^{-/-} fundus with either *iAno1*^{+/-} and (+/+) animals; $n = 4$). Transcripts of *Myh11*, a biomarker for SMCs, were also reduced significantly in fundus muscles of *iAno1*^{-/-} animals compared to *iAno1*^{+/-} and (+/+) muscles. *Myh11* transcripts were decreased 3.69-fold in the fundus of *iAno1*^{-/-} animals compared to *iAno1*^{+/-} (from 5.72 ± 0.18 in *iAno1*^{+/-} to 1.55 ± 0.21 in fundus muscles of *iAno1*^{-/-} animals; $P < 0.001$; $n = 4$). There was no significant difference between *Myh11* transcripts of tamoxifen treated *iAno1*^{+/-} fundus muscles compared to (+/+) muscles (5.71 ± 0.19 ; $P > 0.05$).

We have previously characterized post-junctional neural responses of the gastric fundus of (+/+) mice

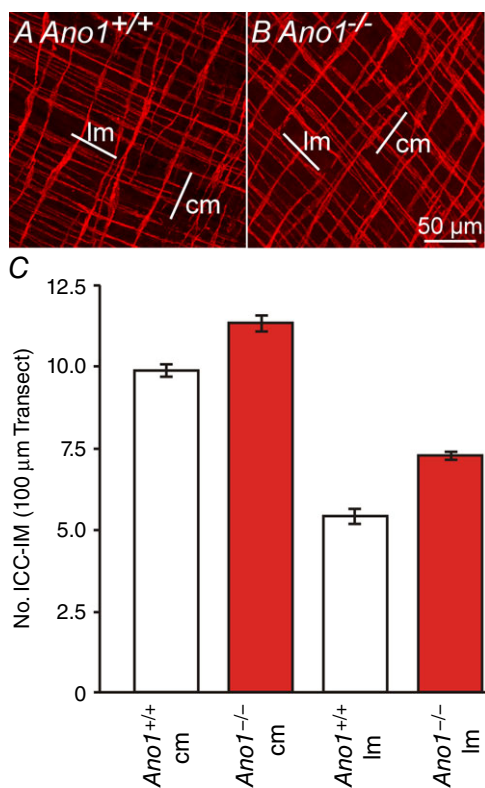


Figure 8. Numbers of Kit⁺ ICC-IM were not different in the gastric fundus of *Ano1*^{+/+} and *Ano1*^{-/-} mice

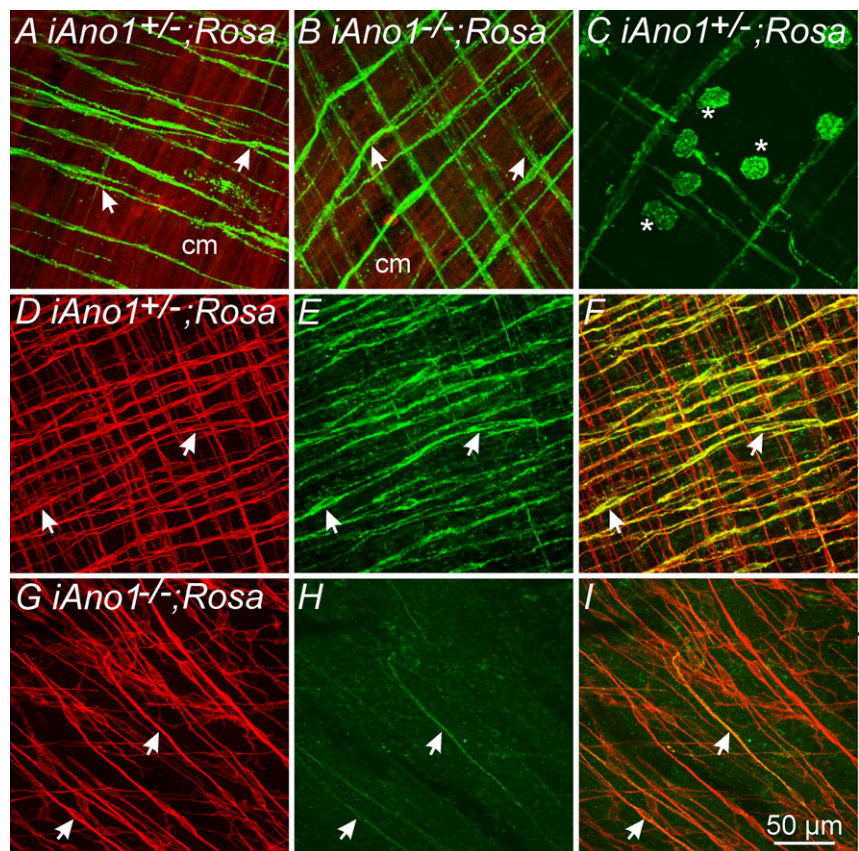
A and B, Kit labelling of ICC-IM in the circular (cm) and longitudinal (lm) muscle layers of a P5 *Ano1*^{+/+} control and an age-matched *Ano1*^{-/-} mutant in two random fields of view. In a 100 μm cross-transection line perpendicular to the respective muscle layer, there was an average of 9.8 ± 0.4 ICC-IM in the cm and 5.4 ± 0.5 ICC-IM in the lm of fundus from *Ano1*^{+/+} controls. In *Ano1*^{-/-} animals, there was an average of 11.3 ± 0.5 ICC-IM in the cm and 7.2 ± 0.2 ICC-IM in the lm, respectively ($n = 5$). C, there was no statistical significant difference between the number of ICC-IM in both muscle layers between *Ano1*^{+/+} controls and *Ano1*^{-/-} mutants (six random fields of view from five *Ano1*^{+/+} and 5 *Ano1*^{-/-} mutants).

(Ward *et al.* 2000; Beckett *et al.* 2002). RMPs in fundus muscles from tamoxifen treated control *iAno1*^{+/-} mice averaged -47.4 ± 1.6 mV and, similar to (+/+) mice, produced continuous small amplitude, noisy oscillations in membrane potential (Fig. 10A–D). EFS (1–20 Hz) evoked frequency-dependent biphasic responses consisting of a transient EJP followed by a more sustained IJP, similar to (+/+) controls. EJPs averaged 1.1 ± 0.5 mV and 1.4 ± 0.6 mV; IJPs averaged 2.0 ± 0.4 mV and 5.8 ± 1.2 mV at 1 pulse and 5 Hz, respectively ($n = 11$; Fig. 10A). In the presence of L-NNA, RMP remained unchanged (-48 ± 1.3 mV) but IJPs were blocked. EJPs increased to 3.2 ± 1 mV at 1 pulse and 3.4 ± 1.1 mV at 10 Hz (Fig. 10B). In the continued presence of L-NNA, neostigmine, as in (+/+) muscles, caused depolarization (-41 ± 1.9 mV; $P < 0.001$ compared to L-NNA) and EFS evoked a transient EJP (i.e. 4.3 ± 0.8 mV at 5 Hz) and a secondary slower depolarization averaging 5.1 ± 0.5 mV and a half-maximal amplitude duration of 9100 ± 114 ms at 5 Hz (Fig. 10C). As in (+/+) controls, atropine restored RMP (to -47.1 ± 1.9 mV) and the EJPs evoked by EFS were inhibited ($P > 0.05$ compared to L-NNA and control) (Fig. 10D). These responses were not qualitatively different from responses previously measured in (+/+) mice (Ward *et al.* 2000).

Fundus muscles of tamoxifen treated *iAno1*^{-/-} mice had RMPs averaging -50.7 ± 1.2 mV ($n = 27$). The small oscillations in membrane potential (STDs or unitary potentials) occurring in (+/+) and *iAno1*^{+/-} muscles but absent in *Ano1*^{-/-} mice were also greatly attenuated in *iAno1*^{-/-} muscles. In 37% (10 of 27) of fundus muscles from these mice, EFS (1–20 Hz) failed to evoke EJPs. In the remaining 63% (17 of 27), there were small responses that averaged 0.8 ± 0.3 and 1.9 ± 0.5 mV; IJPs averaged 1.2 ± 0.4 mV and 5.1 ± 0.8 mV at 1 pulse and 5 Hz, respectively (Fig. 10E). In L-NNA, RMP remained unchanged (-50.5 ± 1.1 mV) and IJPs were inhibited. EJPs increased slightly to 2.7 ± 0.4 mV at 1 pulse and 4.0 ± 0.4 mV at 5 Hz (Fig. 10F). In L-NNA, neostigmine, similar to (+/+) and *iAno1*^{+/-} mice, caused membrane depolarization (-42.2 ± 1.4 mV; $P < 0.0001$ compared to control) and EFS evoked a transient EJP (i.e. 3.7 ± 0.6 and 8.9 ± 2.3 mV at 1 and 5 Hz, respectively). EFS also evoked a secondary slow depolarization that averaged 3.1 ± 0.5 and 11.6 ± 1.5 mV and a half-maximal amplitude duration of 3525 ± 652 and 11564 ± 974 ms at 1 and 5 Hz, respectively (Fig. 10G). As in (+/+) and *iAno1*^{+/-} muscles, atropine repolarized RMP to control levels (-47.7 ± 1.2 mV) and both the EFS evoked EJP and slow depolarization in the presence of neostigmine

Figure 9. eGFP expression reveals tamoxifen induction of Cre-recombinase and recombination efficiency in ICC-IM in the gastric fundus of *iAno1*;Rosa mice

A, induction of eGFP in ICC-IM following tamoxifen treatment in an *iAno1*^{+/-};Rosa control mouse. ICC-IM (arrows, green) are intermingled within the tdTomato-labelled circular muscle layer (cm; red). **B**, Cre-recombinase induction in ICC-IM (arrows) in an *iAno1*^{-/-};Rosa mouse. **C**, tamoxifen induction of eGFP also occurred in rounded Kit⁺ mast cells within the gastric fundus. **D–F**, Kit and Ano1 labelling in the fundus of a tamoxifen treated *iAno1*^{+/-};Rosa control mouse. **D**, Kit⁺ ICC-IM (arrows, red) are found in both circular and longitudinal layers. **E**, double-labelling of Ano1 in ICC-IM (arrows, green). **F**, merged image of (D) and (E) revealing that the majority of Kit⁺ ICC-IM also expressed Ano1 in *iAno1*^{+/-};Rosa mice. **G–I**, Kit and Ano1 labelling in the fundus of a tamoxifen treated *iAno1*^{-/-};Rosa mouse. **G**, Kit⁺ ICC-IM (arrows, red) are present in the circular layer of tamoxifen treated *iAno1*^{-/-};Rosa mice. **H**, double-labelling of Ano1 reveals significant knockdown of Ano1 in ICC-IM (arrows, green). **I**, merged image of (G) and (H) revealing the degree of tamoxifen induced knockdown of Ano1 in ICC-IM in treated *iAno1*^{-/-};Rosa mice. Scale bar = 50 μ m.



were inhibited ($P > 0.05$ compared to control) (Fig. 10H).

Effects of Ano1 knockdown on mechanical responses to fundus muscles

Cholinergic EJPs were lost in *Ano1*^{-/-} mice and in muscles of *iAno1*^{-/-} mice, suggesting that post-junctional electrical responses are generated by ICC-IM and not by SMCs. However, mechanisms involving Ca²⁺ sensitization of the contractile apparatus also contribute to cholinergic responses (Mori *et al.* 2011; Bhetwal *et al.* 2013) and might be mediated directly in SMCs. Therefore, we also investigated contractile responses of fundus muscles evoked by EFS to determine how loss, reduction and block of Ano1 affects excitation–contraction coupling.

Fundus muscles from P5 *Ano1*^{+/+} and *Ano1*^{-/-} mice were relatively small in size and generated contractile responses that were smaller in amplitude than in muscles of adult animals. Nevertheless, experiments

were performed on these muscles to compare motor responses to EFS. Because the muscle tissues were delicate, only short durations (1 s) were tested (i.e. 1–20 Hz, 0.3 ms pulses). Under control conditions, EFS evoked frequency-dependent contractile responses in *Ano1*^{+/+} muscles, averaging 0.03 ± 0.02 mN at 1 Hz and 0.09 ± 0.04 mN at 10 Hz (Fig. 11A). Contractile responses to EFS in muscles of *Ano1*^{-/-} mice averaged 0.01 ± 0.01 mN and 0.04 ± 0.04 mN at 1 Hz and 10 Hz, respectively. Possibly as a result of the masking of responses by inhibitory neurotransmitters, responses to EFS were not statistically significant ($P > 0.5$) under control conditions in the two groups of animals. After addition of L-NNA (100 μM), contractile responses were enhanced in *Ano1*^{+/+} but not in *Ano1*^{-/-} muscles. For example, contractions of *Ano1*^{+/+} fundus muscles averaged 0.18 ± 0.06 mN and 0.33 ± 0.12 mN at 1 and 10 Hz, respectively (Fig. 11C), and responses to EFS of *Ano1*^{-/-} muscles averaged 0.01 ± 0.01 mN at 1 Hz and 0.05 ± 0.02 mN at 10 Hz ($P < 0.05$ when comparing

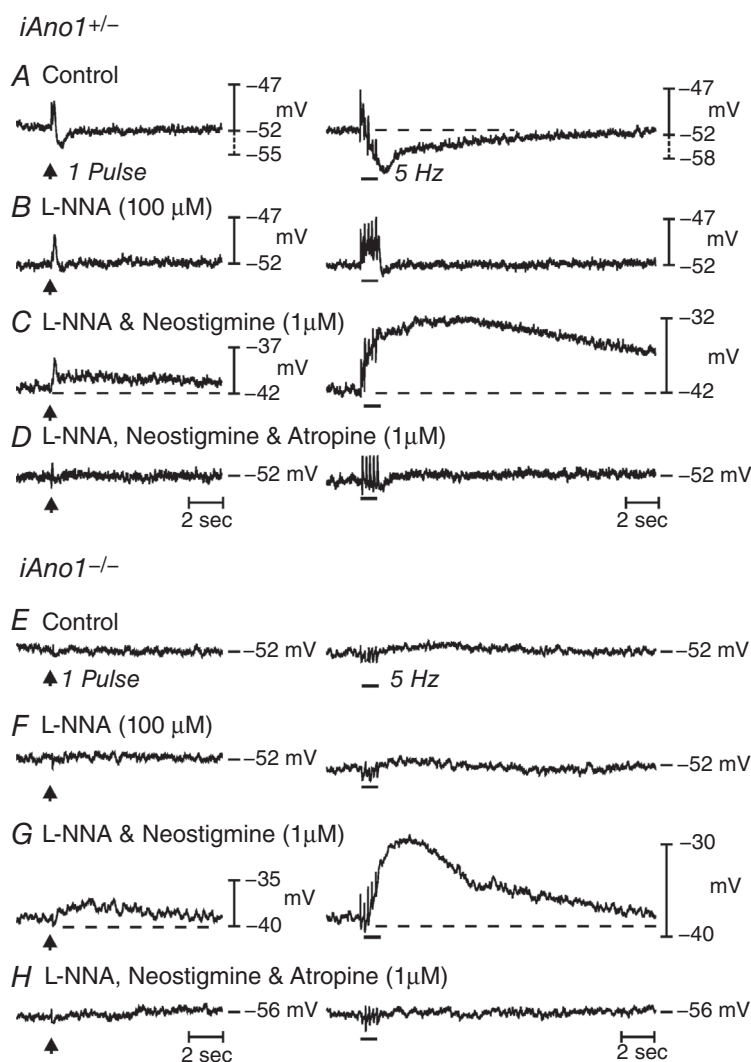


Figure 10. Post-junctional neural responses in tamoxifen treated adult *iAno1*^{+/+} control and an *iAno1*^{-/-} animals

A–D, responses to EFS (1 pulse delivered at arrows; 5 Hz delivered at horizontal bars) of a gastric fundus from a tamoxifen treated *iAno1*^{+/+} animal. A, under control conditions, EFS evoked a frequency-dependent biphasic neural response consisting of a transient EJP followed by a more sustained IJP (dashed line; $n = 11$). B, L-NNA (100 μM) inhibited the IJP at 1 and 5 Hz. C, in the presence of L-NNA and neostigmine (1 μM), EFS caused a depolarization in membrane potential and produced a EJP followed by a large and sustained frequency-dependent depolarization in membrane potential (dashed lines). D, atropine (1 μM) inhibited the EFS evoked EJP and the slow sustained depolarization in membrane potential caused by neostigmine. E–H, EFS evoked neural responses of the gastric fundus from a tamoxifen treated *iAno1*^{-/-} animal. E, under control conditions, EFS evoked little or no post-junctional responses at 1 or 5 Hz ($n = 27$). F, L-NNA (100 μM) did not alter the EFS responses observed under control conditions. G, in the presence of L-NNA, neostigmine (1 μM) produced membrane depolarization and EFS evoked a large and sustained frequency-dependent depolarization in membrane potential (dashed lines). H, atropine (1 μM) repolarized membrane potential and inhibited the EFS evoked sustained depolarization in membrane potential at all frequencies of EFS tested.

Ano1^{+/+} and *Ano1*^{-/-} tissues at 1 and 10 Hz, respectively) (Fig. 11F). Neostigmine (1 μ M), in the continued presence of L-NNA, further increased contractile responses evoked by EFS in both animal groups and there was no

statistical difference in the responses at all frequencies tested. At 1 Hz contractions of *Ano1*^{+/+} tissues averaged 0.33 ± 0.09 mN and at 10 Hz $0.74.2 \pm 29$ mN, whereas, in *Ano1*^{-/-} muscles, contractions averaged 0.33 ± 0.18 mN

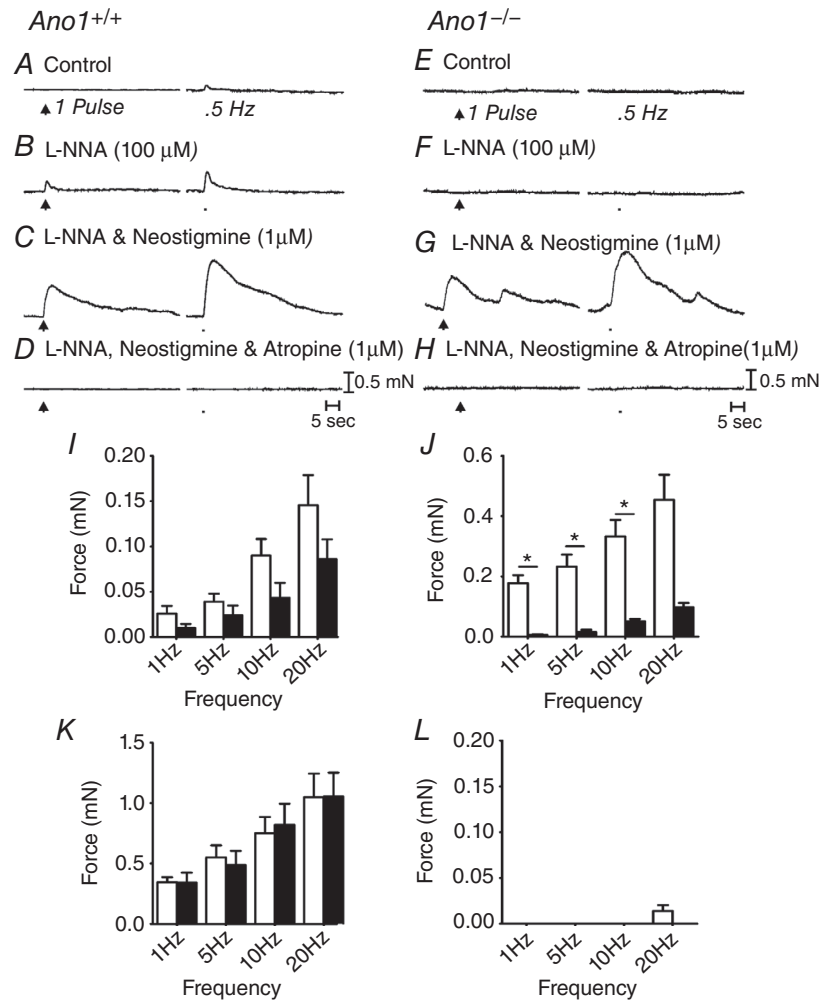


Figure 11. Neurally evoked mechanical responses to EFS of gastric fundus muscles from P5 *Ano1*^{+/+} control and an *Ano1*^{-/-} sibling

Gastric fundus motor responses at the stage of development were small. A–D, motor responses to EFS (1 pulse and 5 Hz for 1 second; arrows and bars respectively) of an *Ano1*^{+/+} gastric fundus. A, under control conditions with no drugs added, neural responses at this developmental age were predominantly excitatory. B, L-NNA (100 μ M) increased the amplitude of EFS evoked contractions at all frequencies tested. C, addition of neostigmine (1 μ M) in the presence of L-NNA produced a marked increase in the nerve evoked contractile responses at all frequencies tested. D, in the continued presence of L-NNA and neostigmine, atropine (1 μ M) abolished EFS evoked contractions. E–H, motor responses to EFS of a P5 *Ano1*^{-/-} gastric fundus. E, little or no contractile responses were observed under control conditions. F, L-NNA (100 μ M) did not reveal excitatory contractile responses. G, in the continued presence of L-NNA, after the addition of neostigmine (1 μ M), EFS evoked contractile responses markedly increased in amplitude and these were similar to *Ano1*^{+/+} tissues. H, atropine (1 μ M) in the presence of L-NNA and neostigmine abolished EFS evoked contractions. I–L, summary of EFS evoked responses of a P5 *Ano1*^{+/+} (white bars; $n = 8$) and *Ano1*^{-/-} mutants (black bars; $n = 15$). I, under control conditions (no drugs), *Ano1*^{-/-} fundus responses were reduced compared to *Ano1*^{+/+} controls but not statistically different. J, in L-NNA, EFS evoked excitatory responses were significantly greater in *Ano1*^{+/+} than *Ano1*^{-/-} mutants at most frequencies tested (* $P < 0.05$, one-way ANOVA). K, in L-NNA, neostigmine markedly increased contractile responses that were not statistically different between *Ano1*^{+/+} and *Ano1*^{-/-} animals. L, neurally evoked contractile responses were inhibited or greatly attenuated by atropine in both animal groups.

at 1 Hz and 0.8 ± 0.38 mN at 10 Hz ($P > 0.05$ when comparing *Ano1*^{+/+} and *Ano1*^{-/-} mutants at both frequencies) (Fig. 11C and G). In the presence of L-NNA and neostigmine, atropine ($1 \mu\text{M}$) blocked excitatory contractile responses at all frequencies (Fig. 11D and H). A summary of the contractile responses of *Ano1*^{+/+} and *Ano1*^{-/-} mutants under different experimental conditions is provided in Fig. 11I–L.

The role of *Ano1* in cholinergic motor responses evoked by EFS was also characterized in muscles from adult animals before and after tamoxifen treatment (i.e. in muscles of *iAno1*^{-/-} and in muscles of *iAno1*^{+/-} controls). Age-matched wild-type (+/+) fundus tissues was also examined for comparison (Fig. 12A–D). EFS (1–20 Hz for 30 s) under control conditions (i.e. absence of antagonists) evoked small excitatory responses followed by dominant inhibitory responses in muscles of *iAno1*^{+/-} mice (Fig. 12E–H). L-NNA ($100 \mu\text{M}$) blocked the inhibitory responses and EFS evoked excitatory responses at all frequencies tested. For example, EFS (5 Hz) evoked tonic contraction averaging 0.66 ± 0.24 mN and, at 20 Hz, the increase in tone averaged 1.81 ± 0.56 mN ($n = 8$) (Fig. 12F). Addition of neostigmine ($1 \mu\text{M}$) in the presence of L-NNA caused an increase in basal tone and a marked increase in the contractions evoked by EFS. At 5 Hz, the amplitude of contractions averaged 5.4 ± 1.1 mN and, at 20 Hz, 9.3 ± 0.8 mN vs. 7.9 ± 1.6 mN (Fig. 12G). Atropine ($1 \mu\text{M}$) inhibited the contractile responses evoked by EFS at all frequencies tested (Fig. 12H). These responses to EFS were essentially similar to that recorded from (+/+) fundus muscles (Fig. 12A–D).

EFS of fundus muscles of *iAno1*^{-/-} mice under control conditions produced smaller amplitude relaxations at all frequencies tested (Fig. 12I). L-NNA ($100 \mu\text{M}$) inhibited the relaxation responses and converted responses to small amplitude tonic contractions that were significantly smaller than those in *iAno1*^{+/-} mice (Fig. 12J). For example, at 5 Hz, the amplitude of contractions averaged 0.27 ± 0.08 mN and, at 20 Hz, the responses averaged 0.70 ± 0.16 mN ($P < 0.05$ and $P < 0.01$ for 5 and 20 Hz, respectively, compared to *iAno1*^{+/-} animals; $n = 20$). As in *iAno1*^{+/-} mice, addition of neostigmine ($1 \mu\text{M}$) in the presence of L-NNA caused an increase in tone and an increase in nerve evoked contractile responses in *iAno1*^{-/-} mice. With neostigmine, there was no significant difference in the amplitude of EFS evoked contractions in *iAno1*^{+/-} controls and *iAno1*^{-/-} mice. At 5 Hz, the amplitude of contractions averaged 5.3 ± 1.1 mN ($P = 0.91$) and, at 20 Hz, 7.9 ± 1.6 mN ($P = 0.54$) compared to *iAno1*^{+/-} mice ($n = 20$) (Fig. 12K). Atropine inhibited contractile responses at all frequencies tested (Fig. 12L). A summary of nerve evoked responses of gastric fundus muscles from tamoxifen treated *iAno1*^{+/-} controls and *iAno1*^{-/-} mutants is provided in Fig. 12M–P.

Pharmacological effects on EJPs of wild-type muscles

Pharmacological studies were also performed to further test the role of *Ano1* in cholinergic excitatory responses. The small molecule *Ano1* channel blocker benzbramarone, as recently identified by high-throughput screening, was tested (Huang *et al.* 2012) because this compound inhibited CCh-induced CaCC in isolated ICC-IM (Fig. 5) and was also recently shown to inhibit pacemaker activity in the stomach and small intestine (Hwang *et al.* 2016). Generation of slow waves in these organs are a result of activation of *Ano1* (Hwang *et al.* 2009).

Benzbramarone (1 – $5 \mu\text{M}$) dose-dependently inhibited EJPs. For example, EJP amplitude averaged 7.2 ± 1.5 mV (in L-NNA; $100 \mu\text{M}$) at 1 Hz and 12.5 ± 1.8 mV at 20 Hz and was reduced to 0.3 ± 0.3 mV at 1 Hz and 8.7 ± 1.9 mV at 20 Hz in the presence of $5 \mu\text{M}$ benzbramarone ($P < 0.01$ for both frequencies; $n = 7$) (Fig. 13A–E). Benzbramarone also caused membrane hyperpolarization at concentrations of $3 \mu\text{M}$ or greater (i.e. from -45.4 ± 1.2 mV to -51.3 ± 1.4 mV at $3 \mu\text{M}$ $P < 0.001$ and to -58.7 ± 1 mV at $5 \mu\text{M}$; $P < 0.001$). The effects of benzbramarone on EJPs and membrane potential are summarized in Fig. 13F).

Mechanical responses elicited by EFS were also sensitive to benzbramarone. The dominant response of adult gastric (+/+) fundus muscles to EFS under control conditions (i.e. absence of drugs) was excitation followed by relaxation at 1 Hz and relaxation followed by excitation at higher frequencies. Relaxations were abolished by L-NNA ($100 \mu\text{M}$), unmasking frequency-dependent, atropine-sensitive contractions. Contractile responses evoked by EFS (1–10 Hz; 30 s) in the presence of L-NNA were dose-dependently inhibited by benzbramarone. Neural responses were attenuated at $1 \mu\text{M}$ (Fig. 14C) and almost completely blocked at 3–5 μM ($n = 6$) (Fig. 14D and E). Benzbramarone also caused a dose-dependent reduction in basal tone. Tone was reduced 0.73 ± 0.2 mN at $1 \mu\text{M}$, 1.54 ± 0.4 mN at $3 \mu\text{M}$ and 1.64 ± 0.4 mN at $5 \mu\text{M}$. When neurally evoked responses to EFS were inhibited in benzbramarone ($5 \mu\text{M}$), exogenous ACh ($1 \mu\text{M}$) still caused contraction of fundus muscles (Fig. 14F). A summary of the effects of benzbramarone on responses to EFS is provided in Fig. 14G ($n = 7$).

Discussion

In the present study, we investigated whether ICC-IM or SMCs primarily receive and transduce inputs from cholinergic motor neurons. This has been a subject of controversy for several years (Ward *et al.* 2000; Huizinga *et al.* 2008; Goyal & Chaudhury 2010; Sarna 2008; Zhang *et al.* 2011; Sanders *et al.* 2010, 2014a; 2016) and part of the conflicting information may be a result of compensatory

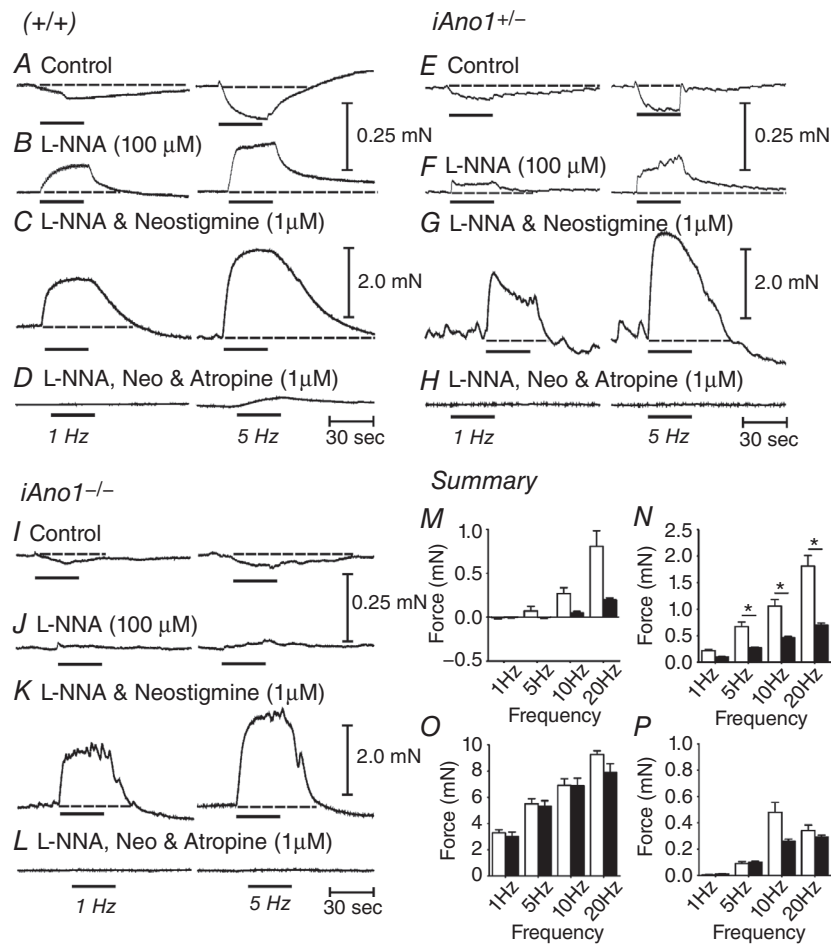


Figure 12. Neurally evoked mechanical responses of gastric fundus muscles from (+/+), *iAno1*^{+/-} control and *iAno1*^{-/-} animals

A–D, typical mechanical responses from a (+/+) animal to demonstrate similarity in responses of tamoxifen treated *iAno1*^{+/-} fundus muscles. A, under control conditions (no drugs), EFS (1–20 Hz for 30 s; 0.3 ms pulses) produced predominant relaxations at 1 Hz (left; horizontal bar) and a slight contraction followed by relaxation at 5 Hz (right; horizontal bar; dashed lines). B, in the presence of L-NNA (100 μ M), nerve evoked inhibitory responses to EFS were converted to excitatory responses at all frequencies tested. C, addition of neostigmine (1 μ M) in the continued presence of L-NNA caused an increase in basal tone and spontaneous contractile activity. EFS in the presence of neostigmine evoked large contractile motor responses at 1 and 5 Hz (dashed lines). D, excitatory motor responses were inhibited by atropine (1 μ M) at 1 Hz and greatly attenuated at 5 Hz. E–H, mechanical responses to EFS of a tamoxifen treated *iAno1*^{+/-} fundus were similar to (+/+) muscles ($n = 8$). E, under control conditions, EFS evoked an initial slight contraction followed by sustained relaxation at 1 and 5 Hz. F, in the presence of L-NNA (100 μ M), inhibitory responses were converted to excitatory responses at all frequencies tested. G, after addition of neostigmine (1 μ M) in the continued presence of L-NNA, there was an increase in spontaneous contractile activity and EFS evoked large contractile motor responses at 1 and 5 Hz. H, excitatory motor responses were inhibited by atropine (1 μ M) at all frequencies of EFS tested. I–L, mechanical responses to EFS of a tamoxifen treated *iAno1*^{-/-} fundus muscle. I, EFS evoked only slight relaxation responses at both 1 and 5 Hz. J, in L-NNA (100 μ M), there was reduced excitatory responses compared to (+/+) and *iAno1*^{+/-} control muscles. K, neostigmine (1 μ M) in the continued presence of L-NNA produced large contractile responses similar to (+/+) and *iAno1*^{+/-} fundus muscles. L, atropine added in the presence of L-NNA and neostigmine inhibited EFS evoked contractile responses, suggesting that they were cholinergically mediated responses. M–P, summarized contractile responses of *iAno1*^{+/-} (white bars; $n = 8$) and *iAno1*^{-/-} animals (black bars; $n = 20$). M, EFS evoked responses under control conditions (no drugs added). Both inhibitory and excitatory responses were recorded. N, after addition of L-NNA, EFS evoked excitatory responses were noted in both animal groups; however, the fundus responses of tamoxifen treated *iAno1*^{-/-} animals were reduced significantly ($*P < 0.05$, one-way ANOVA). O, after the addition of neostigmine, contractile responses were markedly increased in both animal groups, and there was no significant difference in responses between both animals. P, after the addition of atropine, there was a marked reduction in EFS evoked responses in gastric fundus muscles from both animal groups.

mechanisms that sustain, but modify, cholinergic neurotransmission in mice with congenital loss of ICC (Bhetwal *et al.* 2013). We found that different types of ionic conductances are activated by cholinergic stimulation of ICC-IM and SMCs. SMCs are known to express NSCC responsive to muscarinic agonists in GI SMCs of many

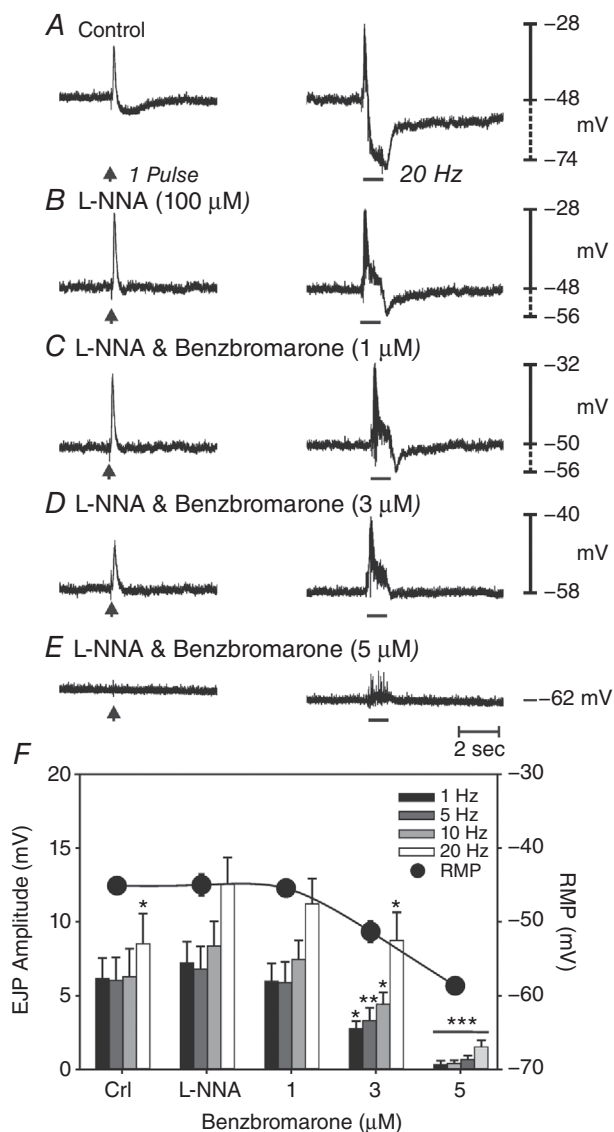


Figure 13. Effects of benzbromarone on neurally evoked EJPs of (+/+) fundus muscles

Responses to 1 Hz (arrow; left) and to 20 Hz (horizontal bars, right), 0.3 ms in duration for 1 s. *A*, under control conditions, prominent EFS evoked EJPs were followed by smaller, more slowly developing IJPs. *B*, L-NNA (100 μM) inhibited IJPs and potentiated the amplitude of EJPs. *C* and *D*, benzbromarone (1–3 μM) caused a reduction in EFS evoked EJPs. *E*, EJPs were inhibited at a concentration of 5 μM. Benzbromarone also caused hyperpolarization in membrane potential. *F*, summary of the effects of benzbromarone on EJPs (1–20 Hz) and membrane potential (solid circles; $n = 7$; * $P < 0.05$; ** $P < 0.01$; *** $P < 0.001$, one-way ANOVA).

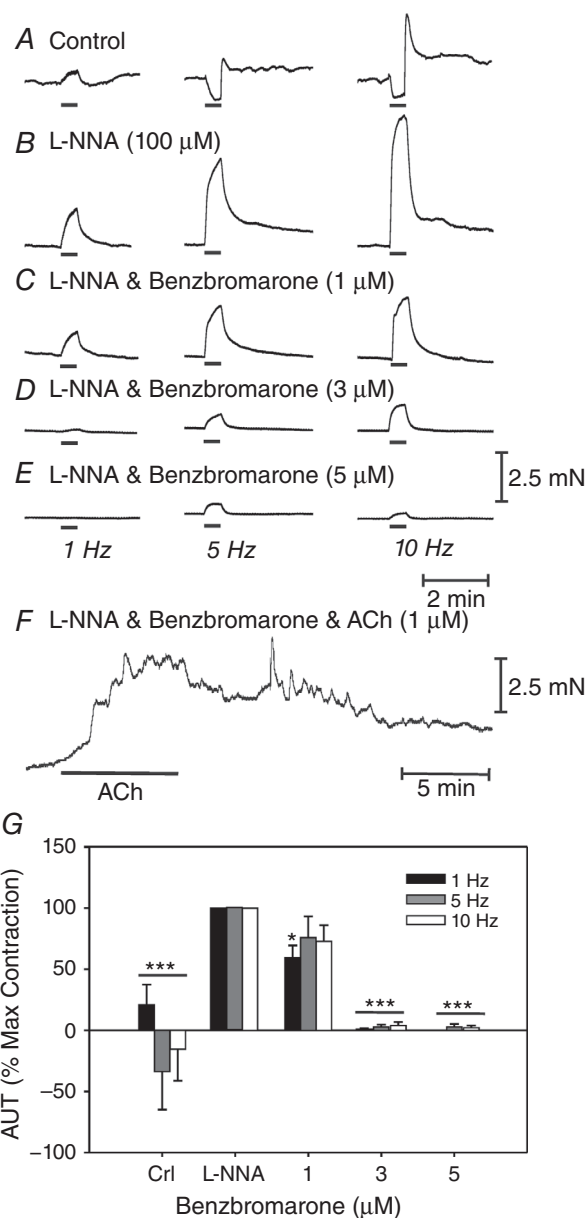


Figure 14. Inhibition of neurally evoked mechanical responses but not ACh responses in adult (+/+) fundus muscles by benzbromarone

A, under control conditions, EFS (0.3 ms in duration for 30 s; 1 Hz, left traces; 5 Hz, middle traces; 10 Hz, right traces, delivered at the horizontal bars) evoked mixed contractions (1 Hz) and relaxations (5 and 10 Hz) followed by excitation. *B*, in L-NNA (100 μM), EFS evoked neural responses were converted to pronounced excitatory responses. *C–E*, benzbromarone (1–5 μM) significantly reduced or blocked EFS evoked contractile responses. *F*, although benzbromarone (5 μM) greatly reduced or abolished EFS evoked neural responses, it did not inhibit excitatory responses evoked by exogenous application of ACh (1 μM). *G*, summary of the dose-dependent inhibition of benzbromarone on EFS evoked responses ($n = 7$; * $P < 0.05$; *** $P < 0.001$, one-way ANOVA).

organs and species (Benham *et al.* 1985; Lim & Bolton, 1988; Inoue & Isenberg, 1990a; Vogalis & Sanders, 1990; Sims, 1992; Lee *et al.* 1993; Zholos & Bolton, 1997). As shown in the present study, ICC-IM express CaCC, and this conductance was not resolved in fundus SMCs. The CaCC is probably encoded by *Ano1*, a gene that is highly expressed in ICC throughout the GI tract (Chen *et al.* 2007; Lee *et al.* 2017) and translated to protein labelled by immunohistochemical techniques (Blair *et al.* 2012; Gomez-Pinilla *et al.* 2009; Hwang *et al.* 2009; Cobine *et al.* 2017). We reasoned that, if post-junctional electrical responses (EJPs) were compromised in animals made null for *Ano1*, this would be strong support for the innervation of ICC-IM by cholinergic motor neurons and, if post-junctional electrical and mechanical responses were reduced or blocked in fundus muscles of *Ano1*^{-/-} mice, this would suggest that ICC-IM are the dominant post-junctional cell receiving and transducing inputs from cholinergic enteric motor neurons in wild-type muscles. These hypotheses were confirmed by the results obtained in the present study.

We investigated the conductance and cells responsible for mediating post-junctional responses to cholinergic, excitatory neurotransmission in the murine gastric fundus. Fundus muscles were chosen for these experiments because they have no ongoing slow wave activity that can obscure EJPs. In rhythmic portions of the GI tract, activation of cholinergic neurons initiates premature slow waves, and EJPs cannot be distinguished from the upstroke of the slow wave (Beckett *et al.* 2003). Fundus muscles also have only a single class of ICC (ICC-IM) that is found to be intermingled and closely associated with motor neurons in bundles of SMCs (Burns *et al.* 1996; Sanders, 1996; Ward *et al.* 2000). Distinct membrane conductances were activated in ICC-IM and SMCs by muscarinic agonists and we used this basic observation to determine which cells are activated in fundus muscles by ACh released from motor neurons. A Cl⁻ conductance was activated in ICC-IM, and, as above, this is probably a result of the expression of *Ano1*. Expression of *Ano1* was not resolved in SMCs and antagonists of this conductance failed to inhibit the inward currents elicited by CCh in these cells. Many previous studies report that NSCC are activated by muscarinic stimulation of GI SMCs (Benham *et al.* 1985; Lim & Bolton, 1988; Inoue & Isenberg, 1990a; Vogalis & Sanders, 1990; Sims, 1992; Lee *et al.* 1993; Zholos & Bolton, 1997) and such a conductance was activated by CCh in SMCs of murine fundus. CCh generated an outwardly rectifying current that reversed at 0 mV and was blocked by lanthanum.

A study of small intestinal longitudinal tissues and SMCs also concluded that the conductance activated by muscarinic stimulation is the result of an NSCC encoded by *Trpc4* and *Trpc6* genes (Tsvilovskyy *et al.* 2009). When both genes were deactivated, excitatory,

cholinergic responses of small intestinal muscles to EFS were reduced, suggesting that the NSCC composed of TRPC4 and TRPC6 channel proteins is essential for transducing cholinergic neurotransmission. These findings contrast with the observations of the present study in which blockers of *Ano1* reduced cholinergic responses in ICC-IM, but not in SMCs, and cholinergic EJPs and contractile responses in intact muscles of the fundus were reduced in *Ano1* knockouts and by *Ano1* channel blocking drugs. Differences in the anatomy and innervation of the fundus and longitudinal muscle layer of the small intestine may explain the differences in mechanisms mediating post-junctional muscarinic responses. In fundus, ICC-IM are closely associated with varicosities of enteric motor neurons, which are the presumed sites of neurotransmitter release (Burns *et al.* 1996; Ward *et al.* 2000) in both the circular and longitudinal muscle layers (Fig. 2). Previous studies have suggested that this close relationship between nerve processes and ICC-IM tends to restrict overflow of ACh to SMCs as a result of the high expression of AChE by motor neurons (Worth *et al.* 2015; Bhetwal *et al.* 2013). In the mouse and other laboratory rodents, ICC-IM are not present in the longitudinal muscle layer of the small intestine (Torihashi *et al.* 1995; Burns *et al.* 1997) and innervation appears to be indirect, possibly resulting from overflow of neurotransmitter from the tertiary plexus of neurons connecting myenteric ganglia (Richardson, 1958; Llewellyn-Smith *et al.* 1993). However, most regions of the GI tract, particularly in larger mammals (Horiguchi *et al.* 2003; Blair *et al.* 2012) and humans (Ibba Manneschi *et al.* 2004), display the anatomical arrangements of motor neurons entwined with the cells of the SIP syncytium and close associations between ICC and varicosities of motor neurons, as found in the fundus. Thus, the murine fundus may be a more stereotypical example for motor innervation and neurotransmission in the GI tract than in intestinal longitudinal muscle layers of laboratory rodents.

CCh evoked large amplitude currents in ICC-IM that reversed near the Cl⁻ equilibrium potential were inhibited by *Ano1* antagonists, and not affected by La³⁺, suggesting that activation of a Cl⁻ conductance is the primary post-junctional response that would be activated if ICC-IM mediate responses activated by ACh released from motor neurons. This idea was tested with intact muscles in which we could observe post-junctional electrical and mechanical responses to EFS. EJPs and contractile responses were generated in fundus muscles; however, when *Ano1* was knocked out in global *Ano1*^{-/-} animals or knocked down by tamoxifen activation of Cre recombinase in mice with double-floxed *Ano1* alleles (*iAno1*^{-/-}), EJPs and contractile responses were reduced (inducible knockout mice) or abolished (global knockout mice). Our results are consistent with the hypothesis that ICC-IM, via expression of muscarinic receptors (Epperson *et al.* 2000) and coupling to activation of *Ano1* channels,

elicits most of the post-junctional response to enteric excitatory regulation of the fundus.

Previous studies using W/W^V mice in which ICC-IM are developmentally repressed as a result of loss-of-function mutations in the tyrosine kinase activity of Kit, suggested a role for ICC-IM in enteric motor neurotransmission (Burns *et al.* 1996; Ward *et al.* 2000). These experiments used short duration stimuli to allow clear evaluation of junction potentials, whereas contractile experiments, performed in later studies using longer duration EFS, concluded that ICC are not necessary for nitrergic and/or cholinergic neurotransmission (Huizinga *et al.* 2008; Zang *et al.* 2010, 2011). After comparing contractile responses to EFS with the actual lesions in ICC in the muscles under investigation, we more recently found that fundus muscles of W/W^V mice are not completely devoid of ICC, as previously assumed (Sanders *et al.* 2014b). Mice with profound depletion of ICC displayed loss of nitrergic inhibition (1–32 Hz of EFS), although nitrergic responses were maintained in mice retaining portions of the ICC-IM population. However, it was also interesting to note that contractile responses to cholinergic nerve stimulation could be augmented in muscles with reduced ICC populations (Sanders *et al.* 2014b).

Genetic manipulation of pathways involved in neuro-effector responses is a powerful means of determining the cells and mechanisms responsible for neurotransduction. However, global knockouts can produce confusing results because, throughout development, there are opportunities for compensatory processes to replace normally utilized mechanisms. Cell-specific conditional knockout approaches such as expression of inducible Cre recombinase driven by cell-specific promoters can improve on the selectiveness of gene deactivation and reduce the time available for compensation of natural mechanisms. However, studies have shown that knockdowns produced by iCre can yield less than a complete knockout of floxed alleles (Bao *et al.* 2013). Thus, remaining functional phenotypes can persist and be confusing in terms of the true function and importance of specific pathways. For example, a recent study utilized Cre/LoxP technology to investigate the role of *Ano1* in pacemaker activity of small intestinal ICC in the myenteric plexus (Malysz *et al.* 2017). Quantitative PCR demonstrated only an ~50% reduction in *Ano1* transcripts after tamoxifen treatment, and immunohistochemistry revealed a mosaic pattern of *Ano1* protein in ICC-MY. Partial loss of *Ano1* did not block pacemaker activity but, instead, resulted in slow waves of diminished duration; however, slow waves were either desynchronized or lost entirely in animals showing extensive reduction in *Ano1*. In the present study, we utilized both global knockouts of *Ano1* and inducible knockdowns using the Cre/loxP approach. We found total loss of cholinergic electrical and mechanical responses in the global knockouts, although

in only 37% of muscles were cholinergic responses absent in the inducible knockdowns of *Ano1*. The remaining mice showed reduced responses. These findings, however, should not be interpreted as supporting the likelihood of additional ion channels contributing to cholinergic responses in the tamoxifen treated animals because cholinergic responses were abolished in global knockouts and in muscles treated with pharmacological antagonists of *Ano1*. Furthermore, although fundus muscles of *iAno1*^{-/-} mice showed a -4.3-fold reduction in *Ano1* transcripts, they were still detected. Tamoxifen treatment probably had no indirect effect on *Ano1* transcript expression because there was no significant difference in expression between tamoxifen treated *iAno1*^{+/-} and age-matched (+/+) mice.

The SIP syncytium is an integrated tissue that determines the excitability of SMCs and ultimately the nature of GI motility (Sanders *et al.* 2012). We found that knockdown of *Ano1* in *iAno1*^{-/-} animals led to a significant reduction in the expression of genes associated with the three cell types making up the SIP syncytium, including *Myh11* (SMCs), *Kit* (ICC) and *Pdgfra* (*Pdgfra*⁺ cells). Although SIP cells are now known to interact on a moment-to-moment basis to regulate the excitability of SMCs, the present study also suggests that regulation of SIP cell phenotypes may also be interdependent. *Ano1* has been identified as a regulator of cell proliferation, migration and differentiation, as well as being involved in cell apoptosis (Wanitchakool *et al.* 2014). Our observation that these gene transcripts were down regulated in SMCs and *Pdgfra*⁺ cells needs further investigation. *Kit* was also down regulated in *iAno1*^{-/-} animals, although this did not lead to a marked change in protein expression, suggesting that there may be a significant time-dependence in the reduction of *Kit* transcript expression *vs.* *Kit* protein in ICC. Interestingly, although *Ano1* was not expressed in *Ano1*^{-/-} mutants *Kit* expression in ICC appeared normal.

The results of the present study and those of a previous study assaying post-junctional Ca²⁺ sensitization pathways activated by cholinergic neurotransmission (Bhetwal *et al.* 2013) suggest that ICC-IM are the primary mediators of cholinergic neurotransmission. Both studies provide no evidence that ACh released from motor neurons reaches receptors on SMCs under normal circumstances. There is no question that SMCs of the GI tract express muscarinic receptors and respond to cholinergic agonists applied to external solutions (also known as bath application) and so the question of why it is difficult to resolve responses in SMCs to cholinergic neurotransmission remains. Many investigators have assumed that neurotransmitters released from enteric motor neurons can diffuse freely and bind to receptors distributed throughout the smooth muscle syncytium (*i.e.* *en passant*

innervation and volume transmission). Indeed, the close contacts made between nerve varicosities and ICC-IM may restrict the diffusion of ACh and a high concentration of the neurotransmitter in confined post-junctional volumes may facilitate rapid metabolism as a result of expression of AChE by enteric neurons (Worth *et al.* 2015). Thus, the 'length constant of effectiveness' of ACh released from nerve varicosities may be limited. Data from the present study and the results of a previous study (Bhetwal *et al.* 2013) support this idea by showing that: (i) reduced ICC-IM in *W/W^V* mice resulted in the activation of Ca²⁺ mechanisms in SMCs in response to cholinergic neurotransmission that were not activated when ICC-IM were present in wild-type mice and (ii) an inhibitor of AChE caused recruited Ca²⁺ sensitization mechanisms in SMCs and evoked large amplitude, long duration electrical and mechanical responses to EFS in fundus muscles that were not affected by genetic deactivation of *Ano1*.

In summary, *Ano1* transcripts and protein are expressed functionally in ICC-IM that lie in close association with varicose nerve processes of cholinergic motor neurons in the gastric fundus. Cholinergic stimulation of isolated ICC-IM caused activation of a Cl⁻ conductance, presumed to be *Ano1* because these channels are expressed in ICC-IM and the responses were blocked by *Ano1* antagonists. CCh activated a NSCC in SMCs. Blocking *Ano1*, either by genetic deactivation or by *Ano1* channel antagonists, significantly decreased EJPs and contractile responses in intact fundus muscles. Our data are consistent with the hypothesis that ACh released from motor neurons primarily binds to receptors on ICC-IM and does not reach muscarinic receptors expressed by SMCs. Transduction of inputs from cholinergic motor neurons and development of EJPs occur via activation of *Ano1* channels expressed by ICC-IM. Depolarization responses are conveyed to SMCs via gap junctions, and depolarization of SMCs activates voltage-dependent Ca²⁺ channels, Ca²⁺ entry, Ca²⁺ sensitization mechanisms mediated by protein kinase C, and phosphorylation of CPI-17 and contraction (Bhetwal *et al.* 2013; Jensen *et al.* 1996; Somlyo & Somlyo, 2003). Blocking ACh metabolism or disrupting the close connectivity between nerve varicosities and ICC-IM causes activation of secondary responses mediated by SMCs. This redundancy in responsiveness may be a safety mechanism to insure continued GI motility in animals with defects in ICC or a vestigial response left over from before ICC became critical components of the SIP syncytium with respect to regulating GI motility.

References

- Bao J, Ma HY, Schuster A, Lin YM & Yan W (2013). Incomplete cre-mediated excision leads to phenotypic differences between *Stra8-iCre*; *Mov10l1*(lox/lox) and *Stra8-iCre*; *Mov10l1* (lox/ Δ) mice. *Genesis* **51**, 481–490.
- Beckett EA(1), Horiguchi K, Khoyi M, Sanders KM & Ward SM (2002). Loss of enteric motor neurotransmission in the gastric fundus of SI/SI(d) mice. *J Physiol* **543**, 871–887.
- Beckett EA, McGeough CA, Sanders KM & Ward SM (2003). Pacing of interstitial cells of Cajal in the murine gastric antrum: neurally mediated and direct stimulation. *J Physiol* **553**, 545–559.
- Beckett EA, Bayguinov YR, Sanders KM, Ward SM & Hirst GD (2004). Properties of unitary potentials generated by intramuscular interstitial cells of Cajal in the murine and guinea-pig gastric fundus. *J Physiol* **559**, 259–269.
- Beckett EA, Bayguinov YR, Sanders KM, Ward SM & Hirst GD (2004). Properties of unitary potentials generated by intramuscular interstitial cells of Cajal in the murine and guinea-pig gastric fundus. *J Physiol* **559**, 259–69.
- Beckett EA, Takeda Y, Yanase H, Sanders KM & Ward SM (2005). Synaptic specializations exist between enteric motor nerves and interstitial cells of Cajal in the murine stomach. *J Comp Neurol* **493**, 193–206.
- Beckett EA, Sanders KM & Ward SM (2017). Inhibitory responses mediated by vagal nerve stimulation are diminished in stomachs of mice with reduced intramuscular interstitial cells of Cajal. *Sci Rep* **7**, 44759.
- Benham CD, Bolton TB & Lang RJ (1985). Acetylcholine activates an inward current in single mammalian smooth muscle cells. *Nature* **316**, 345–347.
- Bennett MR (1966). Transmission from intramural excitatory nerves to the smooth muscle cells of the guinea-pig taenia coli. *J Physiol* **185**, 132–147.
- Bhetwal BP, Sanders KM, An C, Trappanese DM, Moreland RS & Perrino BA (2013). Ca²⁺ sensitization pathways accessed by cholinergic neurotransmission in the murine gastric fundus. *J Physiol* **591**, 2971–2986.
- Blair PJ, Bayguinov Y, Sanders KM & Ward SM (2012). Interstitial cells in the primate gastrointestinal tract. *Cell Tissue Res* **350**, 199–213.
- Bolton TB & Zholos AV (1997). Activation of M2 muscarinic receptors in guinea-pig ileum opens cationic channels modulated by M3 muscarinic receptors. *Life Sci* **60**, 1121–1128.
- Burns AJ, Lomax AE, Torihashi S, Sanders KM & Ward SM (1996). Interstitial cells of Cajal mediate inhibitory neurotransmission in the stomach. *Proc Natl Acad Sci USA* **93**, 12008–12013.
- Burns AJ, Herbert TM, Ward SM & Sanders KM (1997). Interstitial cells of Cajal in the guinea-pig gastrointestinal tract as revealed by c-Kit immunohistochemistry. *Cell Tissue Res* **290**, 11–20.
- Chen H, Ordög T, Chen J, Young DL, Bardsley MR, Redelman D, Ward SM & Sanders KM (2007). Differential gene expression in functional classes of interstitial cells of Cajal in murine small intestine. *Physiol Genomics* **31**, 492–509.
- Cobine CA, Hannah EE, Zhu MH, Lyle HE, Rock JR, Sanders KM, Ward SM & Keef KD (2017). ANO1 in intramuscular interstitial cells of Cajal plays a key role in the generation of slow waves and tone in the internal anal sphincter. *J Physiol* **595**, 2021–2041.
- Desai KM, Sessa WC & Vane JR (1991). Involvement of nitric oxide in the reflex relaxation of the stomach to accommodate food or fluid. *Nature* **351**, 477–479.

- Dwyer L, Rhee PL, Lowe V, Zheng H, Peri L, Ro S, Sanders KM & Koh SD (2011). Basally activated nonselective cation currents regulate the resting membrane potential in human and monkey colonic smooth muscle. *Am J Physiol Gastrointest Liver Physiol* **301**, G287–G296.
- Edwards FR, Hirst GD & Suzuki H (1999). Unitary nature of regenerative potentials recorded from circular smooth muscle of guinea-pig antrum. *J Physiol* **519**, 235–250.
- Epperson A, Hatton WJ, Callaghan B, Doherty P, Walker RL, Sanders KM, Ward SM & Horowitz B (2000). Molecular markers expressed in cultured and freshly isolated interstitial cells of Cajal. *Am J Physiol Cell Physiol* **279**, C529–C539.
- Faria D, Rock JR, Romao AM, Schweda F, Bandulik S, Witzgall R, Schlatter E, Heitzmann D, Pavenstädt H, Herrmann E, Kunzelmann K & Schreiber R (2014). The calcium-activated chloride channel anoctamin 1 contributes to the regulation of renal function. *Kidney Int* **85**, 1369–1381.
- Gomez-Pinilla PJ, Gibbons SJ, Bardsley MR, Lorincz A, Pozo MJ, Pasricha PJ, Van de Rijn M, West RB, Sarr MG, Kendrick ML, Cima RR, Dozois EJ, Larson DW, Ordog T & Farrugia G (2009). Ano1 is a selective marker of interstitial cells of Cajal in the human and mouse gastrointestinal tract. *Am J Physiol Gastrointest Liver Physiol* **296**, G1370–G1381.
- Gordienko DV & Zholos AV. (2004). Regulation of muscarinic cationic current in myocytes from guinea-pig ileum by intracellular Ca²⁺ release: a central role of inositol 1,4,5-trisphosphate receptors. *Cell Calcium* **36**, 367–386.
- Goyal RK & Chaudhury A (2010). Mounting evidence against the role of ICC in neurotransmission to smooth muscle in the gut. *Am J Physiol Gastrointest Liver Physiol* **298**, G10–G13.
- Groneberg D, Zizer E, Lies B, Seidler B, Saur D, Wagner M & Friebe A (2015). Dominant role of interstitial cells of Cajal in nitrenergic relaxation of murine lower oesophageal sphincter. *J Physiol* **593**, 403–414.
- Grundy D (2015). Principles and standards for reporting animal experiments in The Journal of Physiology and Experimental Physiology. *J Physiol* **593**, 2547–2549.
- Hartzell C, Putzier I & Arreola J (2005). Calcium-activated chloride channels. *Annu Rev Physiol* **67**, 719–758.
- Horiguchi K, Sanders KM & Ward SM (2003). Enteric motor neurons form synaptic-like junctions with interstitial cells of Cajal in the canine gastric antrum. *Cell Tissue Res* **311**, 299–313.
- Huizinga JD, Liu LW, Fitzpatrick A, White E, Gill S, Wang XY, Zarate N, Krebs L, Choi C, Starret T, Dixit D & Ye J (2008). Deficiency of intramuscular ICC increases fundic muscle excitability but does not impede nitrenergic innervation. *Am J Physiol Gastrointest Liver Physiol* **294**, G589–G594.
- Huang F, Zhang H, Wu M, Yang H, Kudo M, Peters CJ, Woodruff PG, Solberg OD, Donne ML, Huang X, Sheppard D, Fahy JV, Wolters PJ, Hogan BL, Finkbeiner WE, Li M, Jan YN, Jan LY & Rock JR (2012). Calcium-activated chloride channel TMEM16A modulates mucin secretion and airway smooth muscle contraction. *Proc Natl Acad Sci USA* **109**, 16354–16359.
- Hwang SJ, Blair PJ, Britton FC, O'Driscoll KE, Hennig G, Bayguinov YR, Rock JR, Harfe BD, Sanders KM & Ward SM (2009). Expression of anoctamin 1/TMEM16A by interstitial cells of Cajal is fundamental for slow wave activity in gastrointestinal muscles. *J Physiol* **587**, 4887–4904.
- Hwang SJ, Basma N, Sanders KM & Ward SM (2016). Effects of new-generation inhibitors of the calcium-activated chloride channel anoctamin 1 on slow waves in the gastrointestinal tract. *Br J Pharmacol* **173**, 1339–1349.
- Iino S, Horiguchi K, Horiguchi S & Nojyo Y (2009). c-Kit-negative fibroblast-like cells express platelet-derived growth factor receptor alpha in the murine gastrointestinal musculature. *Histochem Cell Biol* **131**, 691–702.
- Inoue R & Isenberg G (1990a). Acetylcholine activates nonselective cation channels in guinea pig ileum through a G protein. *Am J Physiol Cell Physiol* **258**, C1173–C1178.
- Inoue R & Isenberg G (1990b). Effect of membrane potential on acetylcholine-induced inward current in guinea-pig ileum. *J Physiol* **424**, 57–71.
- Jensen PE, Gong MC, Somlyo AV & Somlyo AP (1996). Separate upstream and convergent downstream pathways of G-protein- and phorbol ester-mediated Ca²⁺ sensitization of myosin light chain phosphorylation in smooth muscle. *Biochem J* **318**, 469–475.
- Klein S, Seidler B, Kettenberger A, Sibaev A, Rohn M, Feil R, Allescher HD, Vanderwinden JM, Hofmann F, Schemann M, Rad R, Storr MA, Schmid RM, Schneider G & Saur D (2013). Interstitial cells of Cajal integrate excitatory and inhibitory neurotransmission with intestinal slow-wave activity. *Nat Commun* **4**, 1630.
- Kurahashi M, Zheng H, Dwyer L, Ward SM, Koh SD, Sanders KM (2011). A functional role for the 'fibroblast-like cells' in gastrointestinal smooth muscles. *J Physiol* **589**, 697–710.
- Lee HK, Bayguinov O & Sanders KM (1993). Role of nonselective cation current in muscarinic responses of canine colonic muscle. *Am J Physiol Cell Physiol* **265**, C1463–C1471.
- Lee MY, Ha SE, Park C, Park PJ, Fuchs R, Wei L, Jorgensen BG, Redelman D, Ward SM, Sanders KM & Ro S (2017). Transcriptome of interstitial cells of Cajal reveals unique and selective gene signatures. *PLoS ONE* **12**, e0176031.
- Lim SP & Bolton TB (1988). A calcium-dependent rather than a G-protein mechanism is involved in the inward current evoked by muscarinic receptor stimulation in dialysed single smooth muscle cells of small intestine. *Br J Pharmacol* **95**, 325–327.
- Llewellyn-Smith IJ, Costa M, Furness JB & Bornstein JC (1993). Structure of the tertiary component of the myenteric plexus in the guinea-pig small intestine. *Cell Tissue Res* **272**, 509–516.
- Malysz J, Gibbons SJ, Saravanaperumal SA, Du P, Eisenman ST, Cao C, Oh U, Saur D, Klein S, Ordog T & Farrugia G (2017). Conditional genetic deletion of Ano1 in interstitial cells of Cajal impairs Ca(2+) transients and slow waves in adult mouse small intestine. *Am J Physiol Gastrointest Liver Physiol* **312**, G228–G245.
- Namkung W, Phuan PW & Verkman AS (2011). TMEM16A inhibitors reveal TMEM16A as a minor component of calcium-activated chloride channel conductance in airway and intestinal epithelial cells. *J Biol Chem* **286**, 2365–2374.
- Ibba Manneschi L, Pacini S, Corsani L, Bechi P & Fausone-Pellegrini MS (2004). Interstitial cells of Cajal in the human stomach: distribution and relationship with enteric innervation. *Histol Histopathol* **19**, 1153–1164.

- Matsuyama H, Tanahashi Y, Kitazawa T, Yamada M, Komori S & Unno T (2013). Evidence for M2 and M3 muscarinic receptor involvement in cholinergic excitatory junction potentials through synergistic activation of cation channels in the longitudinal muscle of mouse ileum. *J Pharmacol Sci* **121**, 227–236.
- Mori D, Hori M, Murata T, Ohama T, Kishi H, Kobayashi S & Ozaki H (2011). Synchronous phosphorylation of CPI-17 and MYPT1 is essential for inducing Ca(2+) sensitization in intestinal smooth muscle. *Neurogastroenterol Motil* **23**, 1111–1122.
- Pacaud P & Bolton TB (1991a). Calcium entry into guinea-pig jejunum cells after calcium stores depletion. *Zeitschrift für Kardiologie* **80**(Suppl 7), 69–72.
- Pacaud P & Bolton TB (1991b). Relation between muscarinic receptor cationic current and internal calcium in guinea-pig jejunal smooth muscle cells. *J Physiol* **441**, 477–499.
- Rhee PL, Lee JY, Son HJ, Kim JJ, Rhee JC, Kim S, Koh SD, Hwang SJ, Sanders KM & Ward SM (2011). Analysis of pacemaker activity in the human stomach. *J Physiol* **589**, 6105–6118.
- Richardson KC (1958). Electronmicroscopic observations on Auerbach's plexus in the rabbit, with special reference to the problem of smooth muscle innervation. *Am J Anat* **103**, 99–135.
- Rock JR, Futtner CR & Harfe BD (2008). The transmembrane protein TMEM16A is required for normal development of the murine trachea. *Dev Biol* **321**, 141–149.
- Sanders KM (1996). A case for interstitial cells of Cajal as pacemakers and mediators of neurotransmission in the gastrointestinal tract. *Gastroenterology* **111**, 492–515.
- Sanders KM, Hwang SJ & Ward SM (2010). Neuroeffector apparatus in gastrointestinal smooth muscle organs. *J Physiol* **588**, 4621–4639.
- Sanders KM, Koh SD, Ro S & Ward SM (2012). Regulation of gastrointestinal motility – insights from smooth muscle biology. *Nat Rev Gastroenterol Hepatol* **9**, 633–45.
- Sanders KM, Ward SM & Koh SD (2014a). Interstitial cells of Cajal: regulators of smooth muscle function. *Physiol Rev* **94**, 859–907.
- Sanders KM, Salter AK, Hennig GW, Koh SD, Perrino BA, Ward SM & Baker SA (2014b). Responses to enteric motor neurons in the gastric fundus of mice with reduced intramuscular interstitial cells of Cajal. *J Neurogastroenterol Motil* **20**, 171–184.
- Sanders KM, Ward SM, Friebe A (2016). CrossTalk proposal: interstitial cells are involved and physiologically important in neuromuscular transmission in the gut. *J Physiol* **594**, 1507–1509.
- Sarna SK (2008). Are interstitial cells of Cajal plurifunction cells in the gut? *Am J Physiol Gastrointest Liver Physiol* **294**, G372–G390.
- Schreiber R, Faria D, Skryabin BV, Wanitchakool P, Rock JR & Kunzelmann K (2015). Anoctamins support calcium-dependent chloride secretion by facilitating calcium signaling in adult mouse intestine. *Pflügers Arch* **467**, 1203–1213.
- Singh RD, Gibbons SJ, Saravanaperumal SA, Du P, Hennig GW, Eisenman ST, Mazzone A, Hayashi Y, Cao C, Stoltz GJ, Ordog T, Rock JR, Harfe BD, Szurszewski JH & Farrugia G (2014). Ano1, a Ca²⁺-activated Cl⁻ channel, coordinates contractility in mouse intestine by Ca²⁺ transient coordination between interstitial cells of Cajal. *J Physiol* **592**, 4051–4068.
- Sims SM (1992). Cholinergic activation of a non-selective cation current in canine gastric smooth muscle is associated with contraction. *J Physiol* **449**, 377–398.
- Somlyo AP & Somlyo AV (2003). Ca²⁺ sensitivity of smooth muscle and nonmuscle myosin II: modulated by G proteins, kinases, and myosin phosphatase. *Physiol Rev* **83**, 1325–1358.
- Stanich JE, Gibbons SJ, Eisenman ST, Bardsley MR, Rock JR, Harfe BD, Ordog T & Farrugia G (2011). Ano1 as a regulator of proliferation. *Am J Physiol Gastrointest Liver Physiol* **301**, G1044–G1051.
- Tack J, Demedts I, Meulemans A, Schuurkes J & Janssens J (2002). Role of nitric oxide in the gastric accommodation reflex and in meal induced satiety in humans. *Gut* **51**, 219–224.
- Torihashi S, Ward SM, Nishikawa S, Nishi K, Kobayashi S & Sanders KM (1995). c-kit-dependent development of interstitial cells and electrical activity in the murine gastrointestinal tract. *Cell Tissue Res* **280**, 97–111.
- Tsvilovskyy VV, Zholos AV, Aberle T, Philipp SE, Dietrich A, Zhu MX, Birnbaumer L, Freichel M & Flockerzi V (2009). Deletion of TRPC4 and TRPC6 in mice impairs smooth muscle contraction and intestinal motility in vivo. *Gastroenterology* **137**, 1415–1424.
- Vogalis F & Sanders KM (1990). Cholinergic stimulation activates a non-selective cation current in canine pyloric circular muscle cells. *J Physiol* **429**, 223–236.
- van Helden DF, Imtiaz MS, Nurgaliyeva K, von der Weid P & Dosen PJ (2000). Role of calcium stores and membrane voltage in the generation of slow wave action potentials in guinea-pig gastric pylorus. *J Physiol* **524**, 245–265.
- Wanitchakool P, Wolf L, Koehl GE, Sirianant L, Schreiber R, Kulkarni S, Duvvuri U & Kunzelmann K (2014). Role of anoctamins in cancer and apoptosis. *Philos Trans R Soc Lond B Biol Sci* **369**, 1638.
- Ward SM, Beckett EA, Wang X, Baker F, Khoyi M & Sanders KM (2000). Interstitial cells of Cajal mediate cholinergic neurotransmission from enteric motor neurons. *J Neurosci* **20**, 1393–1403.
- Worth AA, Forrest AS, Peri LE, Ward SM, Hennig GW, Sanders KM (2015). Regulation of gastric electrical and mechanical activity by cholinesterases in mice. *J Neurogastroenterol Motil* **21**, 200–216.
- Zhang Y, Carmichael SA, Wang XY, Huizinga JD & Paterson WG (2010). Neurotransmission in lower esophageal sphincter of W/W^u mutant mice. *Am J Physiol Gastrointest Liver Physiol* **298**, G14–G24.
- Zhang RX, Wang XY, Chen D & Huizinga JD (2011). Role of interstitial cells of Cajal in the generation and modulation of motor activity induced by cholinergic neurotransmission in the stomach. *Neurogastro Motil* **23**, e356–371.

- Zholos AV & Bolton TB (1997). Muscarinic receptor subtypes controlling the cationic current in guinea-pig ileal smooth muscle. *Br J Pharmacol* **122**, 885–893.
- Zhu MH, Kim TW, Ro S, Yan W, Ward SM, Koh SD & Sanders KM (2009). A Ca²⁺-activated Cl⁻ conductance in interstitial cells of Cajal linked to slow wave currents and pacemaker activity. *J Physiol* **587**, 4905–4918.
- Zhu MH, Sung IK, Zheng H, Sung TS, Britton FC, O'Driscoll K, Koh SD & Sanders KM (2011). Muscarinic activation of Ca²⁺-activated Cl⁻ current in interstitial cells of Cajal. *J Physiol* **589**, 4565–4582.

Additional information

Competing interests

The authors declare that they have no competing interests.

Author contributions

TSS planned and performed the patch clamp experiments on isolated ICC, analysed data and wrote drafts of the manuscript. SJH performed sharp electrode experiments on whole muscles, analysed data and wrote drafts of the manuscript. SDK planned patch clamp experiments, analysed data and

revised the manuscript. SMW planned genetic crosses, immunofluorescence and sharp electrode experiments, analysed data, and wrote and revised the manuscript. KMS planned and co-ordinated experiments on single cells and whole muscles and wrote and revised the manuscript. YB performed immunofluorescence. JR and DP provided strains of mice and helped with the analysis of data.

Funding

This work was supported by DK57236 to SMW and by P01 DK41315 to KMS, SDK and SMW. Confocal imaging was supported by an equipment grant from the NCRR for the Zeiss LSM510 confocal microscope (1 S10 RR16871). FACS sorting was supported by a COBRE P30 GM110767 Phase III grant.

Acknowledgements

The authors are grateful to Dr Deiter Sauer (Technical University Munich, Germany) and Dr Mike Kotlikoff (Cornell University, Ithaca, NY, USA) for providing mice strains *Kit^{CreERT2Ejb1/+ (Kit-Cre)}* and *B6.Cg-Tg^(Myh11-cre,eGFP)*, respectively; Nancy Horowitz for the help in breeding animals, tamoxifen treatments and genotyping; and Byoung H. Koh and David M. White for FACS sorting.